NJC

ROYAL SOCIETY OF CHEMISTRY

PAPER

View Article Online
View Journal | View Issue

Cite this: *New J. Chem.*, 2024, **48**, 8702

Oxazoline amino acid bioconjugates: one-pot synthesis and analysis of supramolecular interactions†

Marija Bakija, Berislav Perić and Srećko I. Kirin *

This publication describes oxazoline–amino acid bioconjugates **1** capable of supramolecular interactions. The bioconjugates contain three main building blocks: an oxazoline ring, a central aromatic unit and an amino acid substituent. Benzene, naphthalene or anthracene with several substitution motifs was used as the central aromatic unit. Two synthetic pathways to β-amino alcohol precursors **3**–**5** are presented; one-pot synthesis with various coupling reagents is compared to linearly sequenced synthesis using protecting groups. In the final step, a cyclization of precursors **3**–**5** to oxazolines **1** is described. Single crystal X-ray diffraction of seven oxazoline bioconjugates is reported (**1**$_{p}$, **1**$_{m6}$, **1**$_{n2}$, **1**$_{n4}$, **1**$_{n5}$, **1**$_{a}$ and **1**$_{t4}$), with an emphasis on supramolecular interactions in the solid state. The capability of bioconjugates **1** to participate in supramolecular interactions in solution was screened by NMR and CD spectroscopy, varying concentrations, temperatures and solvents. The results obtained by crystallography and spectroscopy were further corroborated by computational results for most interesting bioconjugate **1**$_{t1}$. Computational analysis was performed using a CREST/CENSO protocol. In particular, the free energy of formation, ΔG, as well as mean absolute error (MAE) values and correlations of experimental and GIAO calculated NMR parameters have been compared for **1**$_{t1}$ DFT models of monomers and dimers. These results revealed that for **1**$_{t1}$, the supramolecular dimer ensembles are more stable than monomer ensembles.

Received 1st March 2024,
Accepted 3rd April 2024

DOI: 10.1039/d4nj00995a

rsc.li/njc

Introduction

Oxazolines have already been established as a versatile structural motif; their synthetic pathways, characterization methods and applications have been comprehensively reviewed as early as the 1970s.[1] 2-Oxazolines are particularly good building blocks characterized by predictable structures and modalities as well as straightforward synthetic procedures. 2-Oxazolines can easily be prepared from β-amino alcohols, enabling steric modifications *via* introduction of various substituents on positions of 1- and 4- on the planar and rigid oxazoline ring. It therefore does not come as a surprise that to this date 2-oxazolines have found broad application in numerous catalytic reactions,[2,3] especially BOX-type oxazolines[4] (also bearing the term "privileged"),[5] as hybrid donor-type ligands,[6] and as monomers in the synthesis of numerous polymers.[7,8]

Compounds reported in the literature predominantly contain multiple oxazoline rings, while mono-oxazolines are less explored.[9,10] In addition, published research concerning minimal oxazoline-containing compounds capable of undergoing supramolecular interactions is relatively scarce, pertaining mostly to various coordination compounds[11] relying on complexation to facilitate supramolecular interactions between ligands,[12,13] with applications in catalysis utilizing hydrogen bonding (SupraBox)[14] and π–π stacking[15] to increase the selectivity. Moreover, examples of non-polymers, oxazoline-containing supramolecular assemblies with no coordinative bonds are even fewer,[16] and of these, only a handful are conjugated to biomolecules.[17,18]

Bioconjugates contain a stable covalent link between two molecules, at least one of which is a biomolecule, most often a peptide, a nucleic acid, a carbohydrate, a vitamin or a lipid.[19] Bioconjugates often comprise a combination of properties of all of their structural units, giving rise to an array of molecules which are designed to overcome multiple difficulties in complex target systems. Amino acids and peptides are particularly interesting for bioconjugation as their starting materials are readily available and offer a facile method for incorporating chirality into the structure. In addition, these bioconjugates

Ruđer Bošković Institute, Bijenička cesta 54, HR-10000 Zagreb, Croatia.
E-mail: Marija.Bakija@irb.hr, Srecko.Kirin@irb.hr

† Electronic supplementary information (ESI) available: Synthetic procedures, schemes, comprehensive spectroscopic characterisation and computational details. CCDC 2335938–2335948. For ESI and crystallographic data in CIF or other electronic format see DOI: **https://doi.org/10.1039/d4nj00995a**

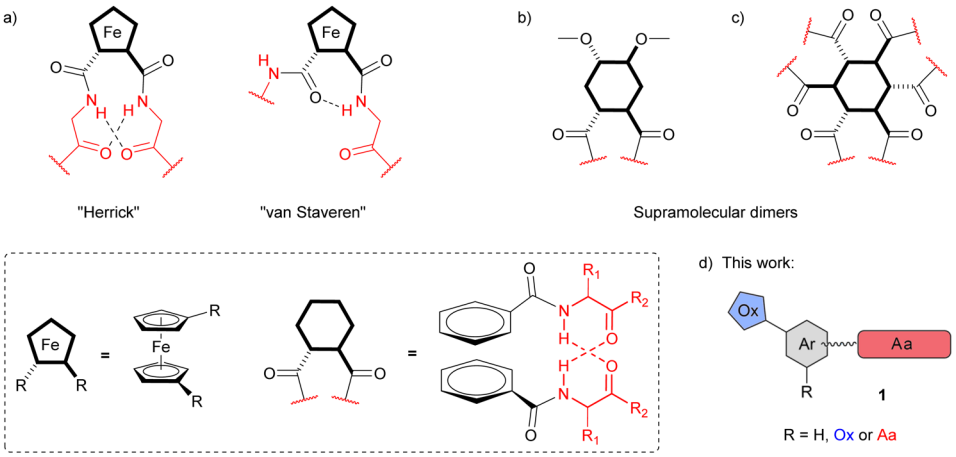

Chart 1 (a) Hydrogen bonding motifs in disubstituted ferrocene peptides; (b) and (c) "Herrick" hydrogen bonding in disubstituted (b) or trisubstituted amino acid bioconjugates (c); top view and side view for both (a) and (b/c) are boxed; the upper ring is indicated in bold. (d) Bioconjugates **1** discussed herein. Ox = oxazoline ring, Ar = central aromatic unit, Aa = amino acid(s).

show a capacity for non-covalent interactions which have been utilized to form non-metal-containing supramolecular systems. Hydrogen bonding motifs of the amino acid strands in 1,2′-disubstituted ferrocene peptides have previously been described (Chart 1a),[20] and ever since, various supramolecular structures bearing one or multiple of these motifs have been studied. Prominent examples include metal containing compounds;[21–24] however, all-organic compounds containing aforementioned H-bonding motifs are known as well. In particular, such organic structures include dimeric structures composed of molecules containing a single (Chart 1b)[25–27] or multiple amino acid substituents (Chart 1c).[28–31]

Oxazoline bioconjugates **1** presented in this study have the capacity to undergo supramolecular interactions (Chart 1d). The three main building blocks of bioconjugates **1**, namely an oxazoline ring (blue), a central aromatic unit (gray) and an amino acid substituent (red), can form a variety of supramolecular interactions: the nitrogen atom of the oxazoline ring can act as a hydrogen bonding acceptor; the central aromatic ring can be involved in aromatic stacking, and the amino acid substituent contains both hydrogen bonding acceptors and donors. Synthetic approaches *via* the one-pot method and *via* protecting groups are compared. The amino alcohol substituents of precursors **3–5** are cyclized to yield a new set of 20 oxazoline–amino acid bioconjugates **1**. The synthesized bioconjugates **1** are then screened for their ability to participate in supramolecular interactions in the solid state using SC-XRD diffraction and in solution using NMR and CD spectroscopies. Selected derivative $\mathbf{1_{t1}}$ was subjected to a detailed computational analysis, from which free energies of formation, ΔG, and NMR parameters were derived to study potential supramolecular interactions.

Results and discussion

Synthesis of intermediates 3

A general approach to oxazoline amino acid bioconjugates **1** involves intermediates **3**, which can be prepared from aromatic dicarboxylic acids **P** as precursors (Scheme 1). Amino acid derivatives **2** and amino alcohol derivatives **4** have been obtained as side products of the one-pot synthesis. In addition to disubstituted aromatic carboxylic acids, trimesic acid was used as a precursor to obtain trisubstituted derivatives of **1–4** (Scheme 1, $R_3 \neq H$). Two approaches to intermediates **3** were considered, namely a one-pot synthesis and a linear synthesis utilizing protecting groups. In the one-pot procedure, the diacid **P** is reacted simultaneously with two different amines (Scheme S1, ESI†). Generally, in this reaction, the expected ratio of the main products is the statistical distribution 1 : 2 : 1, with the higher yield for the mixed product **3**, containing both amines. However, this ratio is rarely obtained experimentally, due to different reactivity and solubility of the amines used.[32–34]

The syntheses of intermediates **3** are divided into several sub-sections below. All obtained intermediates have been characterized by ^{1}H and ^{13}C NMR spectroscopies and ESI mass spectrometry. Additionally, two bis-amino acids ($\mathbf{2_{m1}}$ and $\mathbf{2_{n5}}$), one bis-amino alcohol ($\mathbf{4_{m5}}$) and one mixed derivative ($\mathbf{3_{t3}}$) were characterized by single crystal X-ray diffraction (see Tables S6, S8, S9 and Fig. S13–S18, ESI†).

Synthesis of $\mathbf{3_{m1}}$

For the initial optimization of the one-pot procedure, isophthalic acid was chosen as the diacid precursor, alanine methyl ester as the amino acid and 2-amino-2-methyl-propan-1-ol (AMP) as the amino alcohol. In the first attempt to synthesize the basic compound $\mathbf{3_{m1}}$, the reaction was carried out with the commonly used benzotriazole reagents TBTU/HOBt (Scheme S1 and reaction 1, Table 1, ESI†).[35] However, analysis of the isolated products revealed only the bis-alanine compound $\mathbf{2_{m1}}$, while compounds $\mathbf{3_{m1}}$ and $\mathbf{4_{m1}}$ were not detected. Instead, ester-amide byproducts $\mathbf{6_{m1}}$, $\mathbf{7_{m1}}$ and $\mathbf{8_{m1}}$ formed in trace amounts (Scheme 1b). Obviously, in the course of the reaction, the free alcohol group(s) in $\mathbf{3_{m1}}$ and $\mathbf{4_{m1}}$ can be further derivatized by the TBTU/HOBt protocol. Similarly, if DCC was

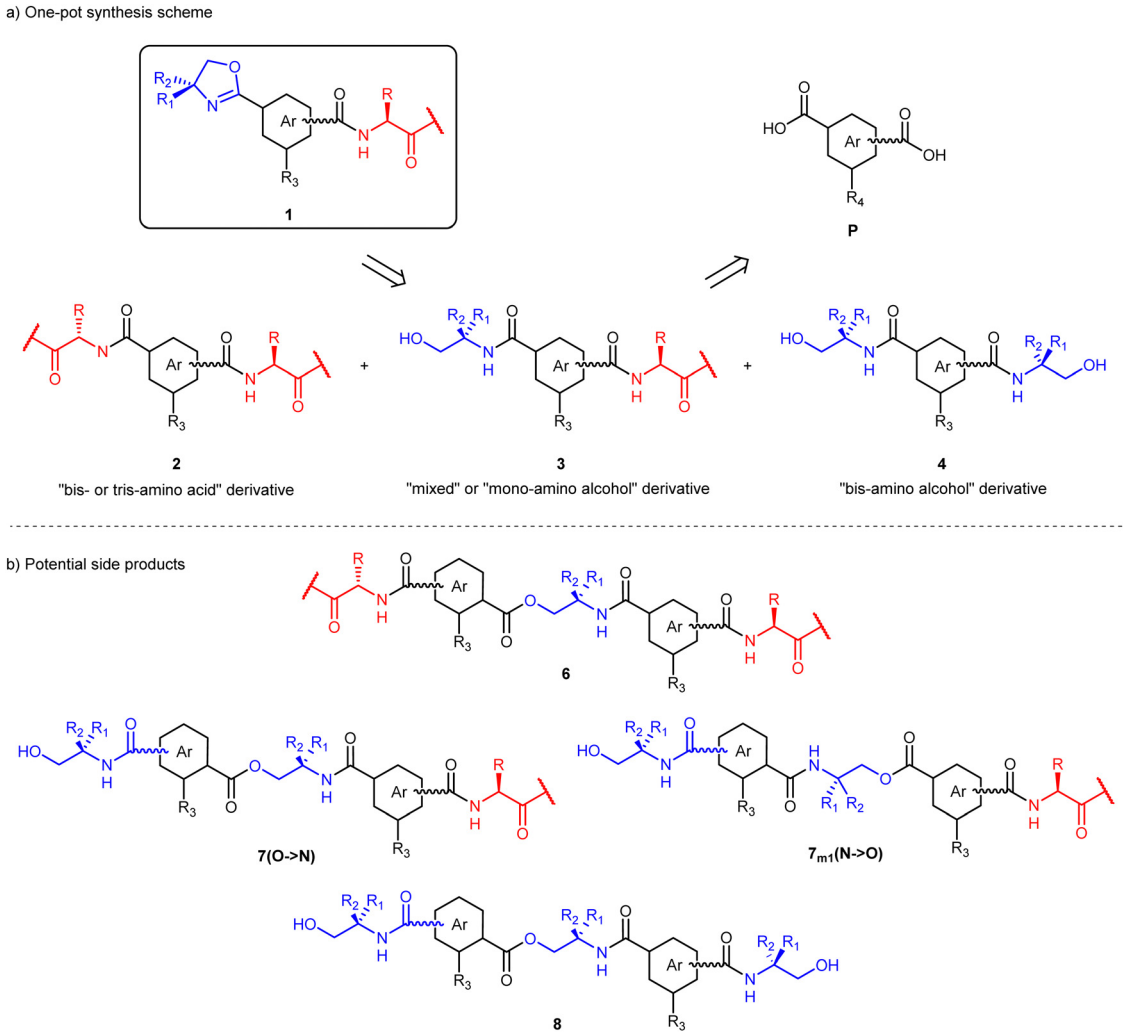

Scheme 1 (a) Disconnection scheme with general structures of oxazoline amino acids **1**, intermediates **2**, **3** and **4** and precursors **P**. (b) Potential side products of the one-pot reaction, obtained by esterification. R_3 = H, amino acid or amino alcohol. R_4 = H or –COOH.

Table 1 One pot reactions with isophthalic acid, H-Ala-OMe and AMP, varying coupling reagents and solvents

Reaction	Coupling reagent	Solvent	Yield (%) (comp.)
1	TBTU/HOBt	DCM	1 ($\mathbf{2_{m1}}$) 8 ($\mathbf{6_{m1}}$) 4 ($\mathbf{7_{m1}}$) 2 ($\mathbf{8_{m1}}$)
2	DCC	DCM	—
3	pyAOP	DMF	17 ($\mathbf{3_{m1}}$)
4	COMU	DMF	25 ($\mathbf{2_{m1}}$) 13 ($\mathbf{3_{m1}}$)
5	HATU	DCM	20 ($\mathbf{2_{m1}}$) 15 ($\mathbf{3_{m1}}$)
6[a]	HATU	DCM	27 ($\mathbf{4_{m1}}$)

[a] Only AMP was used.

used as a coupling reagent (reaction 2, Table 1), the desired derivative $\mathbf{3_{m1}}$ was not obtained.

In order to obtain $\mathbf{3_{m1}}$ as well as to suppress the ester bond formation, other coupling reagents were explored (reactions 3–5, Table 1). In particular, reactions with pyAOP and COMU were performed in DMF, while DCM was used as a solvent for the reaction with HATU. Considering the similarity of yields of $\mathbf{3_{m1}}$ obtained with all three successful coupling reagents ($\eta \sim 15\%$), HATU was used in the following reactions in order to avoid product isolation from DMF.

Since the bis-amino alcohol product $\mathbf{4_{m1}}$ was not isolated in reactions 1–5, a direct attempt with isophthalic acid and two equivalents of AMP was performed, using the same procedure with HATU (reaction 6, Table 1). In this reaction, $\mathbf{4_{m1}}$ was isolated with 27% yield. We note that $\mathbf{4_{m1}}$ was highly insoluble in all solvents except for the particularly polar ones (MeOH, DMSO) and could be filtered off from the reaction solution. No such precipitation was observed in any of the reactions 1–5.

The linear approach to obtain the intermediate $\mathbf{3_{m1}}$ was explored by using protecting groups (Scheme S2, ESI†). The overall yield was 9%, after five steps including two isolations by column chromatography, which is lower than the yield obtained by the one-pot procedure (15%). Considering the

invested amount of time and materials in comparison to the one-pot synthesis, the linear synthesis sequence was not pursued further for simple disubstituted derivatives.

One-pot synthesis of other bis-derivatives 3

First, isomers of phthalic acid as the central aromatic unit have been considered (Table 2 and Chart S1, ESI†). Variations in the type and the number of amino acids and amino alcohols as well as the type and substitution motif of the central aromatic unit have been used.

In reaction 7, *p*-substituted terephthalic acid was used as the central aromatic unit (Table 2). In this reaction, despite the use of HATU, an ester-amide byproduct $\mathbf{6_p}$ was present (Scheme 1b and Chart S5, ESI†). Moreover, it was not possible to separate the desired mixed product $\mathbf{3_p}$ from $\mathbf{6_p}$ by column chromatography. However, $\mathbf{6_p}$ was separated after the cyclization of $\mathbf{3_p}$ to the corresponding oxazoline (see the Oxazoline Synthesis section).

In reactions 8–12, isophthalic acid was used as the central aromatic unit, while alanine methyl ester, phenylalanine methyl ester or the -Gly–Val–Phe-OMe tripeptide was used as the amino acid component and AMP, 2-amino-1-ethanol, valinol, phenylalaninol and phenylglycinol were used as the amino alcohols (Table 2 and Chart S2, ESI†). When the syntheses of compounds $\mathbf{3_{m1}}$ and $\mathbf{3_p}$ are compared to those of compounds $\mathbf{3_{m2}}$–$\mathbf{3_{m6}}$ it can be seen that switching either the alanine amino acid or/and the AMP amino alcohol to derivatives with a bulkier, more hydrophobic group allowed for easier chromatographic isolation of target compounds. For $\mathbf{3_{m6}}$, the corresponding bis-phenylglycinol product $\mathbf{4_{m5}}$ was not separated by chromatography due to too similar chromatographic properties; comparable with $\mathbf{3_p}$, the separation was performed after cyclization to the corresponding oxazolines (see below). The peptide amino acid sequence for the $\mathbf{3_{m6}}$ derivative was chosen according to previously reported compounds containing the same sequence.[23,36]

Furthermore, the central aromatic unit was expanded from benzene to naphthalene or anthracene (reactions 13–18, Table 3 and Chart S3, ESI†). In particular, four naphthalene derivatives (with 1,4-; 1,5-; 2,6-; and 2,7- substitution patterns, respectively) and one anthracene derivative (with 9,10-substitution) were prepared. Bis-amino alcohols $\mathbf{4_{n3}}$ and $\mathbf{4_{n4}}$ that precipitated in reactions 11 and 12, respectively, have been filtered off from the reaction solution. The highest yields have been obtained for intermediates $\mathbf{3_{n1}}$ and $\mathbf{3_{n4}}$, 36% and 33%, respectively. The focus was on the synthesis of intermediates **3**; therefore, no further attempts to synthesize other derivatives **4** were made. During the activation of the anthracene carboxylic acid groups, precipitation occurred even before the addition of amines (reaction 18, Table 3). To avoid loss of reagent before the reaction, in a second attempt, amines were added as soon as 9,10-anthracene dicarboxylic acid and HATU had visibly dissolved.

Table 3 One-pot reaction of H-Ala-OMe and AMP with naphthalene (Nph) and anthracene (Ant) diacids using HATU (DCM)

Reaction	Ar	Yield (comp.)/%	
13	1,4-Nph	8 ($\mathbf{2_{n1}}$)	36 ($\mathbf{3_{n1}}$)
14[a]	1,4-Nph	17 ($\mathbf{2_{n2}}$)	18 ($\mathbf{3_{n2}}$)
15[b]	1,5-Nph	31 ($\mathbf{2_{n3}}$)	15 ($\mathbf{3_{n3}}$)
16[c]	2,6-Nph	5 ($\mathbf{2_{n4}}$)	33($\mathbf{3_{n4}}$)
17	2,7-Nph	18 ($\mathbf{2_{n5}}$)	23 ($\mathbf{3_{n5}}$)
18	9,10-Ant	19 ($\mathbf{2_a}$)	16 ($\mathbf{3_a}$)

[a] H-Gly-OMe was used. [b] Isolated yield of product $\mathbf{4_{n3}}$ was 17%. [c] Isolated yield of product $\mathbf{4_{n4}}$ was 38%.

Synthesis of tris-derivatives $\mathbf{3_t}$

A series of 1,3,5-substituted benzene derivatives was also prepared (Table 4 and Chart S4, ESI†). In anticipation of purification complexity of one-pot products with 1,3,5-substituted benzene, the linear approach was explored first (Scheme S3, ESI†). Derivatives $\mathbf{3_{t3}}$ and $\mathbf{3_{t4}}$ with amino acids L-phenylalanine and D-phenylalanine, respectively, and phenylglycinol as the amino alcohol were synthesized using protecting groups in a similar fashion as the linear synthesis of $\mathbf{3_{m1}}$ (see above). However, there were significant difficulties with the isolation of carboxylic acid group-containing intermediates. It proved to be more efficient to skip the isolation of $\mathbf{14_{t3}}$ and $\mathbf{16_{t3}}$, and similarly to $\mathbf{3_p}$ and $\mathbf{3_{m6}}$, to isolate the corresponding oxazolines after the cyclization (see below).

Because of the difficult isolation of intermediates in the linear synthesis procedure, we synthesized trisubstituted derivatives $\mathbf{3_{t1}}$, $\mathbf{3_{t2}}$ and $\mathbf{3_{t5}}$ using the two-step, one-pot method (Scheme 2 and Table 4). In contrast to the syntheses of disubstituted derivatives, in the trisubstituted case, the amino acid was added in the first step, while the amino alcohol was added in the second step, in order to avoid the formation of ester-amide byproducts. The ratio of added reagents in the two-step procedure proved to be crucial in facilitating formation of the preferred target compound. In reactions 19 and 20 (Table 4), using a 1 : 1 ratio of amino acid and amino alcohol,

Table 2 One-pot reaction of amino acids and amino alcohols with phtalic acid isomers (Ar) using HATU (DCM)

Reaction	Ar	Amino acid	Amino alcohol	Yield (comp.)/%
7[a]	pC$_6$H$_4$	H-Ala-OMe	2-Amino-2-methyl propanol (AMP)	<13[b] ($\mathbf{3_p}$)
8	mC$_6$H$_4$	H-Phe-OMe	2-Amino-1-ethanol (ETA)	22 ($\mathbf{3_{m2}}$)
9	mC$_6$H$_4$	H-Ala-OMe	Valinol (Val[#])	16 ($\mathbf{3_{m3}}$)
10	mC$_6$H$_4$	H-Ala-OMe	Phenylalaninol (Phe[#])	26 ($\mathbf{3_{m4}}$)
11[c]	mC$_6$H$_4$	H-Ala-OMe	Phenylglycinol (Phg[#])	13 ($\mathbf{3_{m5}}$)
12	mC$_6$H$_4$	H-Gly–Val–Phe-OMe	Phenylglycinol (Phg[#])	<52[d] ($\mathbf{3_{m6}}$)

[a] Isolated yield of product $\mathbf{2_p}$ was 7%. [b] Product contained significant amounts of $\mathbf{6_p}$. [c] Isolated yield of product $\mathbf{4_{m5}}$ was 3%. [d] Product contained significant amounts of $\mathbf{4_{m5}}$.

Table 4 One-pot reaction of amino acids and amino alcohols with trimesic acids (Ar) using HATU (DCM)

Reaction	Amino acid	Amino alcohol	Yield (comp.)/%			
19	H-Ala-OMe	AMP	6 ($\mathbf{2_{t1}}$)	27 ($\mathbf{3_{t1}}$)	10 ($\mathbf{4_{t1}}$)	—
20	H-Gly-OMe	Val#	2 ($\mathbf{2_{t2}}$)	16 ($\mathbf{3_{t2}}$)	6 ($\mathbf{4_{t2}}$)	—
21[a]	H-Phe-OMe	Phg#	—	5 ($\mathbf{3_{t5}}$)	26 ($\mathbf{4_{t5}}$)	5 ($\mathbf{5_{t5}}$)

[a] COMU was used.

the target compounds $\mathbf{3_{t1}}$ and $\mathbf{3_{t2}}$ were successfully synthesized in higher yields than the other one-pot products, respectively. On the other hand, using a 1 : 2 ratio facilitated the formation of compound $\mathbf{4_{t5}}$ with higher yield (reaction 21, Table 4).

Synthesis of derivative $\mathbf{3_b}$

Preparation of the C_2-symmetric derivative $\mathbf{3_b}$, in which two simple $\mathbf{3_m}$-like derivatives are linked by 1,4-diaminobutane, has also been performed (Scheme S4, ESI†). Considering the target product's complexity and all the possible byproducts and their polarities, the one-pot procedure was not attempted. Precursor $\mathbf{11_{m5}}$ was easily synthesized by following the linear synthesis sequence as for compound $\mathbf{11_{m1}}$ (see Scheme S2, ESI†). The methyl ester group was then cleaved to yield compound $\mathbf{12_{m5}}$ and the reaction mixture was used in the next step without purification. Compound **17** was prepared from Boc-Val-OH and 1,4-diaminobutane in high isolated yield. In the next step, cleavage of the Boc-protecting group was performed and the obtained product was used in the next step without isolation. Coupling $\mathbf{12_{m5}}$ and **18** with HATU successfully afforded derivative $\mathbf{3_b}$.

Oxazoline synthesis

A total of 20 oxazolines, divided into five groups, have been synthesized utilizing a method previously described by Gang Xu *et al.*,[34] using DAST in DCM at −78 °C (Scheme 3 and Table S2, ESI†). It was found that the yield could be increased by adding excess DAST to the mixture (up to two equivalents). This is reflected in the results for the two attempts of synthesizing $\mathbf{1_a}$, where with 1 equivalent of DAST the reaction yielded 36% of the product, while with 2 equivalents, it yielded 87%. The isolated yield of $\mathbf{1_{n5}}$ is lower than expected due to difficulties in the separation of oxazoline $\mathbf{1_{n5}}$ and starting material $\mathbf{3_{n5}}$. As mentioned above, several intermediates were subjected to cyclization without purification ($\mathbf{1_p}$, $\mathbf{3_{m6}}$, $\mathbf{14_{t3}}$ and $\mathbf{16_{t3}}$), resulting in lower isolated yields of the corresponding oxazolines. All synthesized oxazolines have been characterized by IR, ^{1}H and ^{13}C NMR spectroscopy and ESI-MS and ESI-HRMS spectrometry.

Structures of oxazolines in the solid state

Single crystals of seven oxazoline bioconjugates have been obtained by diffusion from their respective DCM solutions layered with hexane, namely, two oxazolines with a disubstituted central benzene ring ($\mathbf{1_p}$ and $\mathbf{1_{m6}}$), three naphthalene-based oxazolines ($\mathbf{1_{n2}}$, $\mathbf{1_{n4}}$ and $\mathbf{1_{n5}}$), one anthracene oxazoline ($\mathbf{1_a}$) and one trisubstituted derivative ($\mathbf{1_{t4}}$). X-ray diffraction gave insights into the molecular structure and supramolecular interactions in the solid state; the ORTEP diagrams[37] are shown in Fig. 1, experimental data for the X-ray diffraction studies are listed in Tables S6 and S7 (ESI†) while the packing diagrams are shown in Schemes S12 (ESI†).

The crystal packing of the reported single crystal structures gives insight into intermolecular interactions in the solid state. The main intermolecular interaction in the reported structures is hydrogen bonding; in the discussion below, the Bernstein notation for hydrogen bonding patterns is used.[38] Each individual oxazoline bioconjugate participates in hydrogen bonding forming infinite supramolecular polymeric chains,[39] with oxazoline $\mathbf{1_{t4}}$ as a partial exception (see below). Of all amide hydrogen atoms in these structures, only the glycine amide hydrogen atom in oxazoline tripeptide $\mathbf{1_{m6}}$ does not participate in hydrogen bonding. In several cases, the oxazoline moiety is involved in hydrogen bonding as well. However, only the oxazoline nitrogen atoms participate in the hydrogen bonding, while the oxazoline oxygen atoms are almost never part of hydrogen bonding.[40]

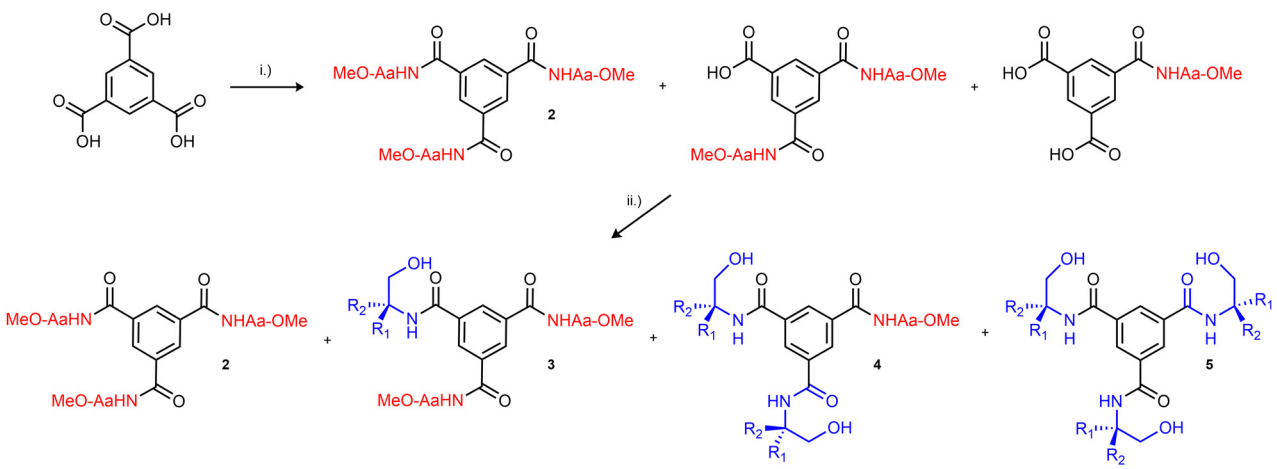

Scheme 2 One-pot synthesis of *t* derivatives (i) amino acid, HATU, DIPEA, DCM, 1 day; (ii) amino alcohol, HATU, DIPEA, 1 day.

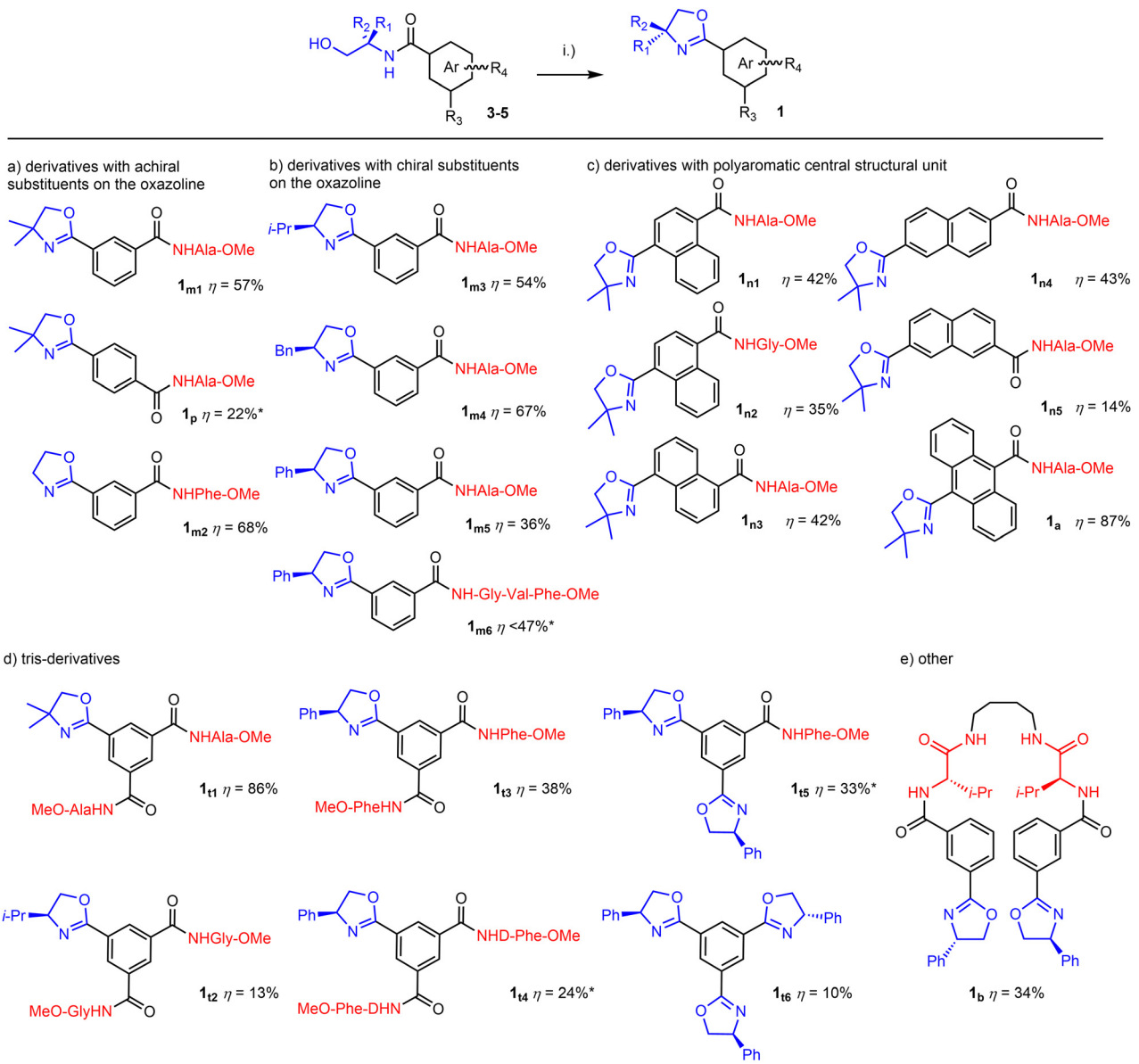

Scheme 3 Oxazoline cyclization reaction. (i) DAST, DCM, K_2CO_3, −78 °C (dry ice in acetone). R_3, R_4 = H, amino acid or oxazoline. *Not chromatographically purified in the previous step(s).

Additionally, there are no structures in which ester atoms participate in hydrogen bonding, and the hydrogen bonding does not occur between separate supramolecular polymeric chains. Characteristic hydrogen bonded secondary structures present in oxazolines **1** are shown in Fig. S9 and S16–S19 (ESI†) and listed in Tables S5 and S9 (ESI†). In particular, four unitary graph set motifs (N_1) appear in the reported structures; chain patterns C(4) and C(9), a finite pattern D and a ring pattern R_2^2(16), while there is also an additional binary graph set motif R_2^2(12), in the structure of oxazoline **1$_{m6}$**. Only one unitary N_1 motif of hydrogen bonding occurs in all structures, apart from the larger oxazolines **1$_{m6}$** and **1$_{t4}$**, which have more than one.

Within the presented structural motifs (Fig. S9, ESI†), in C(4) and R_2^2(12) only amino acids participate in hydrogen bonding, while in C(9) and R_2^2(16), both amino acids and oxazolines are involved. In addition, motif D describes hydrogen bonding of the oxazoline with the methanol solvent in oxazoline **1$_{m6}$**.

Within a polymeric chain, central aromatic units are offset, either in a perpendicular (**1$_p$**, **1$_{n2}$**, **1$_{t4}$**) or in a parallel (**1$_{m6}$**, **1$_{n4}$**, **1$_{n5}$**, **1$_a$**) manner. Therefore, aromatic stacking is not found within the hydrogen bonded chains. However, aromatic stacking[41] is present in two cases, **1$_{n2}$** and **1$_{t4}$**. In oxazoline **1$_{n2}$**, two molecules of neighboring polymeric hydrogen bonded chains interact by aromatic stacking with head-to-tail orientations of oxazoline and amino acid substituents. The distance between centers of the two naphthalene rings in the stack of **1$_{n2}$** is 3.7019(6) Å, while the distance between two naphthalene ring planes is 3.5021(5) Å. Moreover, an aromatic stacking interaction is also present in **1$_{t4}$**. This stacking involves the central aromatic ring of one molecule with the (4*S*)-phenyl oxazoline

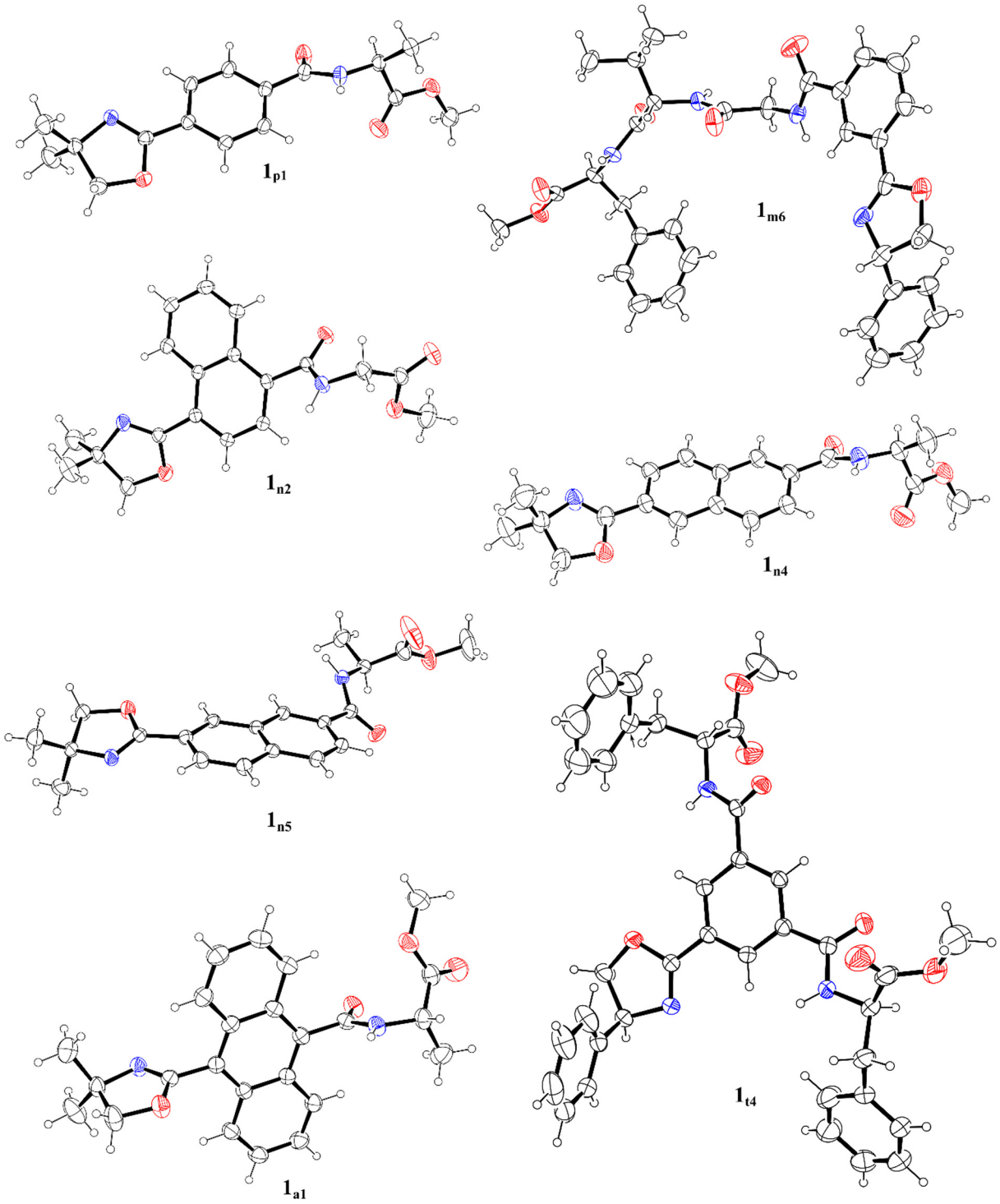

Fig. 1 ORTEP-III drawings[37] with 30% ellipsoid probability level for SCXRD determined structures (complete atom numbering schemes are shown in Fig. S11, ESI†).

substituent from a neighboring molecule. The distance between centers of the two benzene rings is 3.720(2) Å, the shortest contact is 3.130(3) ($H_{Ar\text{-}ox}$–$C_{Ar\text{-}t}$), and the angle between planes of the two benzene rings is 15.7(2)°.

The molecular structure of the oxazoline bioconjugates is dominated by six dihedral angles, α, φ, θ, ϕ, ψ, and χ. The definition of these angles is highlighted in Fig. S10 (ESI†), the corresponding data are collected in Table S6 (ESI†). Structures of similar compounds reported in the literature and the corresponding data are also listed in Table S10 (ESI†). In almost all structures of oxazoline bioconjugates **1** reported herein, the oxazoline double bond and the directly attached amide bond

are nearly co-planar to the central aromatic unit, with a range of angles from 5° to 22° (Table S6, dihedral angles φ and θ, ESI†). Conversely, in the anthracene derivative $\mathbf{1_a}$, the dihedral angles are 93° and 80°, respectively, due to the steric hindrance from neighboring anthracene aromatic hydrogen atoms.

Another finding present in all obtained structures is that the amino acid residues directly attached to the central aromatic unit are bent on the structural backbone ($\chi \sim 90°$) rather than stretched. Even in tripeptide $\mathbf{1_{m6}}$, the χ(Gly–Val) angle is 87°, while χ(Val–Phe) and χ(Phe–ester) angles are 126° and 153°, respectively. This indicates that the tripeptide chain is bent the strongest at the glycine backbone, and gradually transitions into a stretched conformation towards the C-terminal end of the tripeptide.

Supramolecular interactions in solution

^{1}H NMR spectra of all oxazolines **1** and derivatives **2** were measured; their amide hydrogen signals are collected in Table S3 (ESI†). Six oxazolines were selected to be screened for supramolecular interactions using NMR and CD spectroscopy in solution, based on their structural variations, namely $\mathbf{1_{m1}}$, $\mathbf{1_p}$, $\mathbf{1_{m5}}$, $\mathbf{1_{m6}}$, $\mathbf{1_{n4}}$, $\mathbf{1_{t1}}$ and $\mathbf{1_{t5}}$. Their ^{1}H NMR spectra were recorded at concentrations of 6 mM and 60 mM in $CDCl_3$ and 6 mM d_6-DMSO and their CD spectra at 0.06 mM and 0.6 mM in CH_2Cl_2 (Fig. S2–S8, ESI†). The CD results showed that there are no significant intermolecular interactions in solution at concentrations below $c \sim 0.6$ mM, whereas the signal values were too large for the sensitivity of the detector (250–320 nm) at concentrations higher than $c \sim 0.6$ mM. Furthermore, respective hydrogen bond acidity values, A_{NMR},[42–44] were derived from ^{1}H NMR data (Table S4, ESI†); the obtained results confirm that there is no significant hydrogen bonding in dilute solutions.

However, in ^{1}H NMR spectra at 60 mM, N–H chemical shifts of compounds $\mathbf{1_{m6}}$ and $\mathbf{1_{t1}}$ showed concentration dependence in $CDCl_3$, shifting downfield by >0.40 ppm and 0.36 ppm, respectively (Table S4, ESI†). For this reason, oxazolines $\mathbf{1_{m6}}$ and $\mathbf{1_{t1}}$ were chosen for temperature-dependent NMR analysis at c = 60 mM. Spectra were collected every 20 °C in a range from −40 °C to 40 °C (Fig. 2). Individual amide peaks show a difference in the corresponding chemical shift of approximately ~1 ppm at temperatures −40 °C and 40 °C, with the exception of $\mathbf{1_{m6}}$(Val), where the difference is ~0.7 ppm. Calculated temperature-dependent coefficients show that all analyzed amide hydrogen atoms are involved in hydrogen bonding interactions that are strongly affected by temperature, with $\Delta\delta/\Delta T$ values considerably lower than −2.4 ppb K^{-1}(Fig. 2).[45]

Interestingly, several aliphatic peaks shift with the decrease in temperature as well. The ^{1}H NMR peak of the $\mathbf{1_{m6}}$(Val) α-hydrogen atom shifted downfield with the decrease in temperature from 40 °C to −40 °C by 0.34 ppm. More substantial changes can be seen in the temperature-dependent ^{1}H NMR spectra of oxazoline $\mathbf{1_{t1}}$. The two distinct aromatic peaks gradually shift upfield and switch positions with decreasing temperature, indicating weak aromatic stacking interactions. A considerable change to the oxazoline methyl peaks can be seen as well, where the two methyl peaks are not chemically

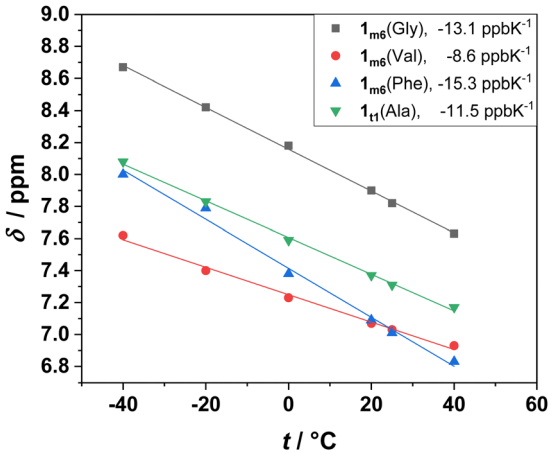

Fig. 2 Temperature dependency of amide hydrogen atom ^{1}H NMR peak shifts in $CHCl_3$ and corresponding amide proton ^{1}H NMR temperature coefficients (ppb K^{-1}, in the upper right corner).

equivalent (Fig. 3, H_b). This lack of equivalency becomes larger with the decreasing temperature, from $\Delta\delta$ = 0.02 ppm to $\Delta\delta$ = 0.11 ppm. It is important to note that this finding has not been detected in any other ^{1}H NMR spectrum of oxazolines derived from the AMP precursor. Additionally, the difference in the chemical shift of each methyl peak of compound $\mathbf{1_{t1}}$ is even smaller at c = 6 mM, with the corresponding value being $\Delta\delta <$ 0.01 ppm. The oxazoline methylene group multiplicity also changes from a singlet to a strongly coupled AB spin system with decreasing temperature (Fig. 3, H_a). These findings indicate that the oxazoline ring faces are not equivalent. Moreover, there is only one set of alanine peaks even at −40 °C, which is in accordance with a conserved pseudo-C_2 symmetry in the supramolecular structure in the solution.

Calculations

Oxazoline bioconjugate $\mathbf{1_{t1}}$, that showed the most interesting supramolecular interactions in solution, was selected for a detailed computational study. Structural ensembles (SE) of $\mathbf{1_{t1}}$ conformers, both monomeric and supramolecularly assembled, were obtained by applying a CREST/CENSO protocol to chosen starting geometries, as suggested by Grimme for

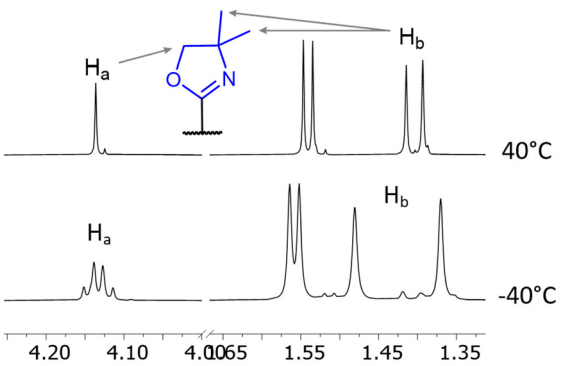

Fig. 3 ^{1}H NMR spectra of $\mathbf{1_{t1}}$ oxazoline in $CHCl_3$ at 40 °C and −40 °C, c = 60 mM.

non-rigid molecules (see Experimental and ESI† for details).[46,47] Ensemble analysis reveals that among the obtained conformers, 29 monomer and 27 dimer $\mathbf{1_{t1}}$ conformers are statistically populated within their respective ensembles (*i.e.* $\Delta G < 2$ kcal mol^{-1}). Cartesian coordinates of individual final $\mathbf{1_{t1}}$ conformers from each obtained monomer and dimer ensemble are collected in two separate files (calc_mono_1t1.xyz, calc_dimer_1t1.xyz), readable with the free-of-charge program Mercury from CCDC.[48]

Within the ensemble of dimer conformers, the dominating supramolecular interactions were found to be hydrogen bonding involving all four amide protons and π–π stacking of the central aromatic units. The hydrogen bonding pattern of the amides found in the dimer ensemble can be divided into five distinct groups: (a) hydrogen bonding with oxazoline nitrogen atom, (b) semi-Herrick conformation, (c) Herrick conformation, (d) hydrogen bonding with the methoxy oxygen and (e) van Staveren conformation (Fig. S20, ESI†). With respect to found hydrogen bonding patterns and relative positions of substituents on the stacked benzene rings, 2 major types of dimers **I** and **II** can be discerned within the ensemble with Boltzmann weight ≥10% (Fig. 4). Data for the types of dimers contributing to the remaining Boltzmann weight of 25% (all the considered dimer conformers make up for 97% of Boltzmann weight) are collected in Fig. S21 and Table S10 (ESI†). The statistically most populated type of dimers was found to be of type **I**, bearing two amide-oxazoline hydrogen bonds (a) and two semi-Herrick hydrogen bonds (b). Interestingly, conformers containing van Staveren hydrogen bonding were found to only make up about 8%. A more detailed description of structural characteristics of dimer ensemble conformers may be found in Fig. S21 and Table S10 (ESI†).

Averaged free energies of the monomer and dimer ensembles were calculated by averaging in accordance with the obtained Boltzmann distribution across respective ensembles for several temperatures (233, 253, 273, 293, 298 and 313 K). The corresponding data are collected as shown in Tables S13 and S14 (ESI†). The free energies of formation, ΔG, calculated from these data show that this model predicts the dimeric structures to be more stable than the monomers at all six temperatures by ≥4.30 kcal mol^{-1} (Table S15, ESI†). Moreover, the free energies of formation gradually decrease in value (*i.e.* increase in absolute value) with the decreasing temperature, suggesting that the dimeric structures are increasingly more stable than monomers at lower temperatures.

For conformers with a Boltzmann population >2% in each structural ensemble, the ^{1}H–^{1}H J couplings and ^{1}H and ^{13}C shieldings were calculated using the GIAO approach.[49] Complete details concerning the procedure of obtaining the final Boltzmann-weighted NMR parameters for each temperature are given in the Experimental part and in the ESI† (Tables S16, S17 and Fig. S24–S27). At low temperatures (233, 253 and 273 K), the calculated shieldings for protons which were experimentally found to be chemically inequivalent were left unaveraged. Fig. S24–S27 (ESI†) show the correlations of the calculated, Boltzmann averaged shieldings (σ_i^c) and experimental shifts (δ_i^o), for monomer and dimer ensembles, respectively. For each correlation, the MAE (mean absolute error) value defined by[50]

$$\mathrm{MAE} = \left(\Sigma_i \left|\delta_i^c - \delta_i^o\right| / N\right) \quad (1)$$

was determined (Table 5); δ_i^c is the calculated chemical shift obtained from the calculated shielding σ_i^c and linear equation obtained from the same correlation calculation. In summation (1), in the correlation calculation and for ^{1}H correlations, only ^{1}H signals coming from protons attached to carbon atoms were used.

From data in Table 5, an opposite trend can be seen in MAE values of monomer and dimer correlations with increased temperature, *i.e.* this model predicts increasingly better compatibility of the dimer model at increasingly lower temperatures, while the monomer model predicts increasingly lower compatibility with the increasingly lower temperatures. Moreover, MAE values for monomeric correlations are generally greater in value than their dimeric counterparts at all temperatures. This is in agreement with the calculated free energies of formation, which was found to favor the dimer over monomer structures at all chosen temperatures.

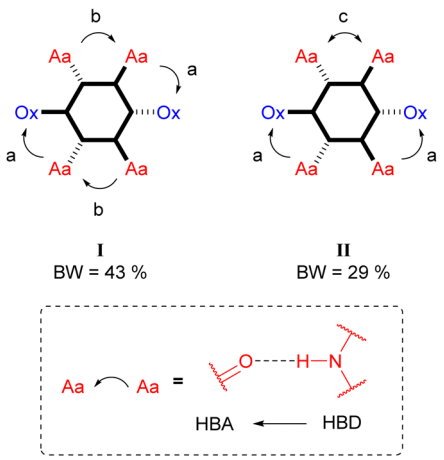

Fig. 4 DFT structures of $\mathbf{1_{t1}}$ dimers **I** and **II** and corresponding hydrogen bonding with Boltzmann weight values greater than 10%. Types of hydrogen bonding: (a) HB with oxazoline, (b) semi-Herrick, and (c) Herrick. The arrowhead indicates the direction of the amide proton donation (each arrowhead on an arrow represents one amide proton). BW = Boltzmann weight, Ox = oxazoline ring, Aa = amino acid, HBA-hydrogen bond acceptor, HBD-hydrogen bond donor.

Table 5 Mean absolute error values of each correlation of the calculated, Boltzmann averaged shieldings (σ_i^c) and experimental shifts (δ_i^o), given in Fig. S24–S26 (ESI)

T/K	MAE (monomer)	MAE (dimer)
233	0.13881	0.0818
253	0.13778	0.08488
273	0.13402	0.08862
293	0.13506	0.09311
298	0.13488	0.0932
313	0.13024	0.10213

Summary

Two synthetic pathways are presented for obtaining derivatives **2–5** and the amino alcohol substituent of the synthesized derivatives is cyclized to afford new oxazoline–amino acid bioconjugates **1**. Generally, the one-pot syntheses proved to be more advantageous for all derivatives **3**, apart from derivative **3b**, for which the linear synthesis was chosen due to the number of constituent building blocks. Different substituents and substitution patterns on the central aromatic unit were used, in order to study their influence on the stacking capabilities of **1** in solution and in the solid state. Single crystal structures showed that all oxazolines participate in hydrogen bonding in the solid state, forming infinite supramolecular polymeric chains.

In contrast, ^{1}H NMR spectra in $CHCl_3$ showed that there are no significant intermolecular interactions in solution at c = 6 mM regardless of the variation of structural elements in disubstituted derivatives with only one amino acid moiety. For larger oxazolines $\mathbf{1_{m6}}$ and $\mathbf{1_{t1}}$, however, NMR spectra at different temperatures showed that these compounds participate in highly temperature-dependent supramolecular interactions at c = 60 mM. The results for tripeptide $\mathbf{1_{m6}}$ suggest that in disubstituted derivatives, more than one amino acid residue is necessary to stabilize supramolecular assemblies. In the case of tris-derivatives substituted with two amino acid moieties, small-non bulky substituents facilitate supramolecular interactions in solution.

In comparison to tris-amino acid compounds,[51,52] which are known to form stacking interactions, we show herein that one amino acid chain can be switched with a small oxazoline building block while preserving the stacking potential. The performed computational studies also support these results, *i.e.* the relative free energy of interaction at all six studied temperatures shows that the dimer ensemble is expected to be more stable than the monomer ensemble ($\geq$4.30 kcal mol^{-1}). Additionally, the MAE values extracted from calculated and measured NMR parameters for the monomer and dimer ensembles show an opposite trend, suggesting better compatibility of the dimer model at lower temperatures and monomer compatibility at higher temperatures. However, the overall MAE values also suggest that the dimer model is generally more compatible than the monomer model, further supporting the experimentally observed results that $\mathbf{1_{t1}}$ molecules participate in supramolecular interactions in solution.

Experimental

General remarks

Reactions were carried out in ordinary glassware and chemicals were used as purchased from commercial suppliers without further purification. All amino acids and amino acid-derived amino alcohols used have L-configuration, unless stated otherwise. All amino acid substituents are denoted with their standard abbreviations, while amino alcohol substituents are, if applicable, denoted with their parent amino acid abbreviation and the hash symbol (*e.g.* Phg$^{\#}$ stands for phenylglycinol). Coupling reagent abbreviations refer to the following compounds: 2-(1*H*-benzotriazole-1-yl)-1,1,3,3-tetramethylaminium tetrafluoroborate (TBTU), 1-hydroxybenzotriazole (HOBt), 1-[bis(dimethylamino) methylene]-1*H*-1,2,3-triazolo[4,5-*b*]pyridinium 3-oxide hexafluorophosphate (HATU), *N*,*N*′-dicyclohexylcarbodiimide (DCC), (7-azabenzotriazol-1-yloxy)tripyrrolidinophosphonium hexafluorophosphate (pyAOP), and (1-cyano-2-ethoxy-2-oxoethylidenaminooxy) dimethylamino-morpholino-carbenium hexafluorophosphate (COMU). The synthesis of compounds **10** and **12** was carried out in a microwave reactor (CEM Discover). Reactions were monitored by TLC on silica gel 60 F_{254} plates and detected with a UV lamp (254 nm); crude products were purified using classic column or flash chromatography. ESI mass spectra were recorded on an HPLC-MS system (Agilent Technologies 1200) coupled using a 6410 Triple-Quadrupole mass spectrometer, operating in a positive ESI mode. High-resolution mass spectra were obtained on a MALDI TOF-TOF instrument using a CHCA matrix. CD spectra were recorded using a spectropolarimeter in 1 cm and 0.1 cm quartz Suprasil cells. Stock solutions of the isolated compounds were prepared for CD measurements of ligands. The measured ellipticity θ [deg] (in CD) is converted to the concentration-independent $\Delta\varepsilon$ [M^{-1} cm^{-1}] through the relation $\Delta\varepsilon = \theta/(l \times 32\,982 \times c)$, where l [cm] is the path length and c [mM] is the concentration. NMR spectra were obtained using a Bruker Avance AV300 or AV600 spectrometer, operating at 300 or 600 MHz for ^{1}H and 75 or 150 MHz for ^{13}C; if not indicated further, the spectra were recorded at room temperature. Chemical shifts, δ (ppm), indicate a downfield shift from the internal standard, tetramethylsilane, TMS. Coupling constants, J, are given in Hz. Individual peaks are marked as singlet (s), doublet (d), triplet (t), quartet (q), quintet (quin.) or multiplet (m). IR spectra were recorded in solid state, using an ATR Agilent Cary 630 FT-IR spectrometer or KBr pellets with a Bruker Alpha FT-IR spectrometer, in the 4000–600 cm^{-1} (ATR) or 4000–350 cm^{-1} (KBr pellets) region.

General peptide coupling procedure in DMF

Isophthalic acid (1 equivalent), L-Ala-OMe·HCl (1 equivalent), AMP (1 equivalent) and DIPEA (4 equivalent) were dissolved in DMF (15 mL) and cooled to 0 °C in an ice bath. Peptide coupling reagent (pyAOP or COMU; 2 equivalents) was added slowly by continuously adding very small portions and stirring was continued overnight. The reaction mixture was then diluted with ethyl acetate (100 mL) and washed with $NaHCO_3$ (sat. aq., 3 × 100 mL), citric acid (10% aq., 3 × 100 mL) and NaCl (sat. aq. 100 mL). The organic phase was dried over Na_2SO_4, filtered and evaporated under reduced pressure to yield the crude product.

General peptide coupling procedure in DCM

Dicarboxylic acid (1 equivalent) was dissolved in DCM (100 mL). Peptide coupling reagent (TBTU/HOBt, HATU or DCC; 1 equivalent) and DIPEA (2 equivalents) were added and stirring was continued for 60 min at room temperature (TBTU/HOBt, HATU).

An amino acid hydrochloride (0.5 equivalent) and amino alcohol (0.5 equivalent) in DCM (10 mL) were added dropwise and stirring was continued for 24 hours. The procedure of adding the coupling reagent, DIPEA and amines were then repeated in the same manner as stated above and stirring was continued for another 24 hours. The reaction mixture was washed with $NaHCO_3$ (sat. aq., 3 × 100 mL), citric acid (10% aq., 3 × 100 mL) and NaCl (sat. aq., 100 mL). The organic phase was dried over $NaSO_4$, filtered and evaporated under reduced pressure to yield the crude product.

Notes

The coupling procedure for trimesic acid was carried out in a similar manner, but with adjusted amounts of reagents used (indicated below in the description of individual reaction), and in each step, only amino acid or amino alcohol was added. Detailed spectroscopic data of precursors from reactions 1–21 can be found in the ESI.†

Reaction 1. Isophthalic acid (2.5 mmol), HOBt (5.0 mmol), TBTU (5.0 mmol), Ala-OMe HCl (2.5 mmol), AMP (2.5 mmol) and DIPEA (10 mmol) were used. Chromatography: 30 g of silica gel, hexane: ethyl acetate = 1 : 1 starting ratio, gradually changed to 1 : 9. Colorless oils $\mathbf{2_{m1}}$ (8.0 mg, 1%) and $\mathbf{6_{m1}}$ (55.5 mg, 4%) were isolated. Fractions containing mixtures of $\mathbf{7_{m1}}$ and $\mathbf{8_{m1}}$ were combined, evaporated and separated by another column chromatography in 4% MeOH in the DCM solvent system. Colorless oils $\mathbf{7_{m1}}$ (94.4 mg, 4%) and $\mathbf{8_{m1}}$ (22.6 mg, 2%) were isolated.

Reaction 2. Isophthalic acid (1.0 mmol), DCC (2 mmol), Ala-OMe HCl (1.0 mmol), AMP (1.0 mmol) and DIPEA (4.0 mmol) were used. A peak of $\mathbf{3_{m1}}$ was absent on the TLC plate after the reaction mixture was layered on and the plate developed.

Reaction 3. Isophthalic acid (1.0 mmol) and pyAOP were used. Chromatography: 30 g of silica gel, 3% MeOH in DCM. Colorless oil $\mathbf{3_{m1}}$ (54.2 mg, 17%) was isolated.

Reaction 4. Isophthalic acid (1.0 mmol), COMU (2.0 mmol), Ala-OMe HCl (1.0 mmol), AMP (1.0 mmol) and DIPEA (4 mmol) were used. Chromatography: 30 g of silica gel, 3% MeOH in DCM. Colorless oils $\mathbf{2_{m1}}$ (83.0 mg, 25%), $\mathbf{3_{m1}}$ (42.3 mg, 13%) and $\mathbf{7_{m1}}$ (24.4 mg, 4%) were isolated.

Reaction 5. Isophthalic acid (2.0 mmol), HATU (4.0 mmol), Ala-OMe HCl (2.0 mmol), AMP (2.0 mmol) and DIPEA (8 mmol) were used. Chromatography: 30 g of silica gel, hexane: ethyl acetate = 2 : 8. Colorless oil $\mathbf{2_{m1}}$ (130.4 mg, 20%) and white solid compound $\mathbf{3_{m1}}$ (97.0 mg, 15%) were isolated.

Reaction 6. Isophthalic acid (0.5 mmol), HATU (1.0 mmol), DIPEA (2.0 mmol) and AMP (1.0 mmol) were used in the same manner as described in the coupling procedure in DCM. After adding the first 0.5 equivalent of AMP, a white powder instantaneously precipitated. After the reaction was finished, the white precipitate was filtered off over blue ribbon filter paper under vacuum and washed with DCM. White solid $\mathbf{4_{m1}}$ (41.8 mg, 27%) was isolated.

Reaction 7. Terephthalic acid (4.0 mmol), HATU (8.0 mmol), Ala-OMe HCl (4.0 mmol), AMP (4.0 mmol) and DIPEA (16.0 mmol) were used. Chromatography: 30 g of silica gel, hexane: ethyl acetate = 25 : 75. White powder $\mathbf{2_p}$ (434.2 mg, 17%), a slightly yellow powder mixture of $\mathbf{3_p}$ and $\mathbf{7_p}$ (184.2 mg in total, 116.1 mg and 59.0 mg, *i.e.* 9% and 5%, respectively, as calculated from NMR).

Reaction 8. Isophthalic acid (4.0 mmol), HATU (8.0 mmol), Phe-OMe HCl (4.0 mmol), ETA (4.0 mmol) and DIPEA (16.0 mmol) were used. After the reaction finished stirring, the white precipitate was filtered off, and the rest of the procedure was carried out with the solution. Chromatography: 30 g of silica gel, 1.5% → 5% MeOH in DCM. White solid $\mathbf{3_{m2}}$ (329.8 mg, 22%) was isolated.

Reaction 9. Isophthalic acid (4.0 mmol), HATU (8.0 mmol), Ala-OMe HCl (4.0 mmol), Val$^{\#}$ (4.0 mmol) and DIPEA (8 mmol) were used. Flash chromatography: 0% → 1% MeOH in DCM. White solid $\mathbf{3_{m3}}$ (236.0 mg, 16%) was isolated. Compound $\mathbf{2_{m1}}$ was detected but not isolated.

Reaction 10. Isophthalic acid (4.0 mmol), HATU (8.0 mmol), L-Ala-OMe HCl (4.0 mmol), Phe$^{\#}$ (4.0 mmol) and DIPEA (16 mmol) were used. Flash chromatography: 0% → 1% MeOH in DCM. White solid $\mathbf{3_{m4}}$ (395.1 mg, 26%) was isolated. Compound $\mathbf{2_{m1}}$ was detected but not isolated.

Reaction 11. Isophthalic acid (4.0 mmol), HATU (8.0 mmol), L-Ala-OMe HCl (4.0 mmol), Phg$^{\#}$ (4.0 mmol) and DIPEA (16 mmol) were used. Chromatography: 30 g of silica gel, 1% → 10% MeOH in DCM. Colorless gum-like solid $\mathbf{3_{m5}}$ (185.2 mg, 13%) was isolated. Compound $\mathbf{2_{m1}}$ was detected but not isolated.

Reaction 12. Isophthalic acid (2.4 mmol), HATU (4.8 mmol), Gly–Val–Phe-OMe (2.4 mmol, prepared according to a known procedure),[23] Phg$^{\#}$ (2.4 mmol) and DIPEA (9.2 mmol) were used. Chromatography: 60 g of silica gel, 5% → 10% MeOH in DCM. Colorless gum-like solid $\mathbf{3_{m6}}$ (753.6 mg, <52%) was found to be contaminated by compound $\mathbf{4_{m5}}$. Compound $\mathbf{2_{m6}}$ was detected but not isolated.

Reaction 13. 1,4-Naphthalene dicarboxylic acid (2.5 mmol), HATU (5.0 mmol), Ala-OMe HCl (2.5 mmol), AMP (2.5 mmol) and DIPEA (10.0 mmol) were used. Chromatography: 30 g of silica gel, hexane: ethyl acetate = 4 : 6, the ratio gradually changed to 3 : 7. White powders $\mathbf{2_{n1}}$ (189.6 mg, 8%) and $\mathbf{3_{n1}}$ (333.0 mg, 36%) were isolated.

Reaction 14. 1,4-Naphthalene dicarboxylic acid (2.0 mmol), HATU (4.0 mmol), Gly-OMe·HCl (2.0 mmol), AMP (2.0 mmol) and DIPEA (8 mmol) and were used. Chromatography: 40 g of silica gel, hexane: ethyl acetate = 2 : 8, the ratio gradually changed to pure ethyl acetate. White powders $\mathbf{2_{n2}}$ (117.6 mg, 17%) and $\mathbf{3_{n2}}$ (134.2 mg, 18%).

Reaction 15. 1,5-Naphthalene dicarboxylic acid (2.0 mmol), HATU (4.0 mmol), Ala-OMe HCl (2.0 mmol), AMP (2.0 mmol) and DIPEA (8 mmol) were used. After adding the second 0.5 equivalent of AMP, a white powder precipitated after some time. When the reaction was finished, the white precipitate was filtered off over blue ribbon filter paper under vacuum and washed with DCM. The white precipitate was confirmed to be $\mathbf{4_{n3}}$ (41.8 mg, 17%) by NMR spectroscopy. Flash chromatography: 2% MeOH in DCM, the ratio gradually changed to 3% MeOH. White powders $\mathbf{2_{n3}}$ (119.9 mg, 16%) and $\mathbf{3_{n3}}$ (113.7 mg, 15%) were isolated.

Reaction 16. 2,6-Naphthalene dicarboxylic acid (2.0 mmol), HATU (4.0 mmol), Ala-OMe HCl (2.0 mmol), AMP (2.0 mmol) and DIPEA (8 mmol) were used. After adding the second 0.5 equivalent of AMP, a white powder precipitated after some time. When the reaction was finished, the white precipitate was filtered off over blue ribbon filter paper under vacuum and washed with DCM. The white precipitate was confirmed to be $\mathbf{4_{n4}}$ (245.9 mg, 38%) by NMR spectroscopy. Chromatography: 2% MeOH in DCM, ratio gradually changed to 10% MeOH. White powders $\mathbf{2_{n4}}$ (34.3 mg, 5%), $\mathbf{3_{n4}}$ (247.1 mg, 33%) and $\mathbf{4_{n4}}$ (31.9 mg, 5%) were isolated.

Reaction 17. 2,7-Naphthalene dicarboxylic acid (2.0 mmol), HATU (4.0 mmol), Ala-OMe HCl (2.0 mmol), AMP (2.0 mmol) and DIPEA (8 mmol) were used. Chromatography: 30 g of silica gel, hexane: ethyl acetate = 1 : 1, the ratio gradually changed to 2 : 8. Yellow $\mathbf{2_{n5}}$ (136.2 mg, 18%) and white $\mathbf{3_{n5}}$ (31.9 mg, 23%) powders were isolated.

Reaction 18. 9,10-Anthracene dicarboxylic acid (1.9 mmol) and HATU were used. Amines were added immediately after the visible dissolution of HATU. Chromatography: 30 g of silica gel, 2% MeOH in DCM. Yellow powders $\mathbf{2_a}$ (150.1 mg, 19%) and $\mathbf{3_a}$ (127.1 mg, 16%) were isolated.

Reaction 19. Trimesic acid (2.0 mmol), HATU (first-day addition: 2.8 mmol, second-day addition: 3.5 mmol), TEA (first-day addition: 12.0 mmol, second-day addition: 12 mmol), L-Ala-OMe HCl (first-day addition: 3.0 mmol), and AMP (second-day addition: 3.5 mmol). Chromatography: 50 g of silica gel, 3.5% → 5% MeOH in DCM. Yellow solids $\mathbf{2_{t1}}$ (159.7 mg, 6%), $\mathbf{3_{t1}}$ (244.8 mg, 27%) and $\mathbf{4_{t1}}$ (87.7 mg, 10%) were isolated.

Reaction 20. Trimesic acid (2.0 mmol), HATU (first-day addition: 2.8 mmol, second-day addition: 3.5 mmol), TEA (first-day addition: 12.0 mmol, second-day addition: 12 mmol), Gly-OMe HCl(first-day addition: 3.0 mmol), and H_2N-Val-OH (second-day addition: 3.5 mmol). Chromatography: 50 g of silica gel, 5% → 8% MeOH in DCM. Light yellow solids $\mathbf{2_{t2}}$ (17.7 mg, 2%), $\mathbf{3_{t2}}$ (138.96 mg, 16%) and $\mathbf{4_{t2}}$ (56.2 mg, 6%) were isolated.

Reaction 21. Trimesic acid (2.0 mmol), COMU (first-day addition: 1.0 mmol, second-day addition: 2.2 mmol), TEA (first-day addition: 4.0 mmol, second-day addition: 8 mmol), L-Phe-OMe HCl (first-day addition: 1.0 mmol), and H_2N-Phegly-OH (second-day addition: 2.2 mmol). Chromatography: 50 g of silica gel, 3% → 5% MeOH in DCM. White solids $\mathbf{3_{t5}}$ (59.0 mg, 5%), $\mathbf{4_{t5}}$ (324.4 mg, 26%) and $\mathbf{5_{t5}}$ (51.9 mg, 5%) were isolated.

Synthesis of derivative 3_b

Phg$^{\#}$-*m*C_6H_4-COOMe ($\mathbf{11_{m5}}$). The same protocol as for compound $\mathbf{11_{m1}}$ was used. HOOC-*m*C_6H_4-COOMe ($\mathbf{10_{m1}}$) (360.3 mg, 2.0 mmol), TBTU (642.2 mg, 2.0 mmol), HOBt (300.2 mg, 2.0 mmol), DIPEA (1. 360 mL, 8.0 mmol), Phg$^{\#}$ (274.4 mg, 2.0 mmol). Chromatography: 30 g of silica gel, 3% MeOH in DCM. NMR spectrum showed a significant content of tetramethyl urea (mass ratio *w*(product) = 89%). Yield: 489.1 mg (1.6 mmol, 73%), white solid. ^{1}H NMR (300 MHz, $CDCl_3$) δ/ppm: 8.43 (t, J = 1.8 Hz, 1H), 8.18 (dt, J = 7.8, 1.5 Hz, 1H), 8.07 (ddd, J = 7.8, 1.9, 1.3 Hz, 1H), 7.60–7.48 (m, 1H), 7.46–7.22 (m, 6H), 6.96 (d, J = 7.1 Hz, 1H), 5.30 (dt, J = 7.2, 4.8 Hz, 1H), 4.03 (dd, J = 6.1, 4.8 Hz, 2H), 3.95 (s, 3H). ^{13}C NMR (75 MHz, DMSO) δ/ppm: 165.87, 165.21, 141.17, 135.11, 132.20, 131.67, 129.73, 128.87, 128.13, 128.03, 127.00, 126.87, 64.41, 56.19, 52.35, 38.24.

Phg$^{\#}$-*m*C_6H_4-COOH ($\mathbf{12_{m5}}$). Phg$^{\#}$-*m*C_6H_4-COOMe ($\mathbf{11_{m5}}$) (440.4 mg, 1.47 mmol) was dissolved in MeOH (20 mL) by using an ultrasonic bath. An aqueous solution of NaOH (117.7 mg, 2.94 mmol in 10 mL of distilled water) was added to the mixture and the reaction mixture was heated in a CEM Microwave Reactor for 20 min (150 W, 50 °C). To the aqueous residue, HCl (247 μL conc., 2.94 mmol in 10 mL of distilled water) was added. Water was evaporated under reduced pressure, the remaining solid mixture dissolved in DCM, and used in the next step without further manipulation.

(Boc-Val-NH-CH_2CH_2)$_2$ (17). A standard coupling procedure with TBTU/HOBt was used. Boc-Val-OH (912.5 mg, 4.20 mmol), TBTU (1348.5 mg, 4.20 mmol), HOBt (643.3 mg, 4.20 mmol), DIPEA (2. 926 mL, 16.80 mmol), and 1,4-diaminobutane (176.3 mg, 2.0 mmol). Chromatography: 30 g of silica gel, 3% MeOH in DCM. Yield: 808.0 mg (1.7 mmol, 83%), colorless oil. ^{1}H NMR (300 MHz, $CDCl_3$) δ/ppm: 6.88 (s, 2H), 5.18 (s, 2H), 3.88 (t, J = 8.0 Hz, 2H), 3.45 (s, 2H), 3.02 (s, 2H), 2.03 (s, 2H), 1.75–1.55 (m, 4H), 1.43 (s, 18H), 0.96 (d, J = 6.7 Hz, 12H). ^{13}C NMR (75 MHz, MeOD) δ/ppm: 174.47, 80.53, 61.78, 39.88, 32.00, 28.71, 27.64, 19.78, 18.55.

(Val-NH-CH_2CH_2)$_2$ (18). (Boc-Val-NH-CH_2CH_2)$_2$ (**17**) (364.98 mg, 0.75 mmol) was dissolved in 10 mL of DCM: trifluoroacetic acid = 1 : 1 solution and stirred for 2 h at room temperature. The solvent was then evaporated under pressure, and the remaining TFA was neutralized with DIPEA (approx. 1.5 mL). The obtained mixture was used in the next step without any further manipulation.

(Phg$^{\#}$-*m*C_6H_4-Val-NH-CH_2CH_2)$_2$ ($\mathbf{3_b}$). A standard coupling procedure with HATU was used. Phg$^{\#}$-*m*C_6H_4-COOH ($\mathbf{12_{m5}}$), (Val-NH-CH_2CH_2)$_2$ (**18**), HATU (870.35 mg, 1.5 mmol), DIPEA (1.041 mL, 6.0 mmol). Chromatography: 30 g of silica gel, 5% MeOH in DCM. Yield: 131.3 mg (0.16 mmol, 21%), white solid. ^{1}H NMR (300 MHz, CD_3OD) δ/ppm: 8.33 (s, 2H), 8.06–7.94 (m, 4H), 7.56 (t, J = 7.8 Hz, 2H), 7.46–7.31 (m, 10H), 5.22 (t, J = 6.6 Hz, 2H), 4.59 (s, 2H), 4.29 (d, J = 8.3 Hz, 2H), 3.87 (d, J = 6.6 Hz, 4H), 2.21–2.08 (m, 2H), 1.58 (s, 4H), 1.00 (dd, J = 8.0, 6.7 Hz, 12H).

Traces of tetramethylurea (TMU) or tri(pyrrolidin-1-yl)phosphine oxide (TPYRPO) were present in some precursors after column chromatography, δ (TMU)/ppm: 2.80 and δ (TPYRPO)/ppm: 3.16, 1.81 in 1H NMR ($CDCl_3$). If there was a significant amount of TMU or TPYRPO present in the samples of precursors, corresponding precursor yields were calculated from their NMR spectra.

General oxazoline synthesis procedure

Diethylaminosulfur trifluoride (1.2 equivalents in 1 mL of dry DCM) was added dropwise to a cooled solution (−78 °C) of precursor (1 equivalent) in dry DCM (14 mL). Additionally, 1 mL of DMF is added to assist dissolution if necessary. After stirring

for 1 h at −78 °C, anhydrous K_2CO_3 (1.5 equivalents) was added in one portion and the mixture was allowed to warm to room temperature. The reaction was quenched with saturated aqueous $NaHCO_3$ (20 mL). The biphasic mixture was extracted with EtOAc (3 × 40 mL). The combined organic extracts were washed with water (100 mL) and NaCl (sat. aq., 100 mL), dried over anhydrous Na_2SO_4 and concentrated.[34]

(Me$_2$-ox)-*m*C$_6$H$_4$-Ala (1$_{m1}$). AMP-*m*C_6H_4-Ala (**3$_{m1}$**) (1.0 mmol). Chromatography: 30 g of silica gel, hexane: ethyl acetate = 7 : 3. Yield: 173.3 mg (0.6 mmol, 57%), colorless oil. M_r ($C_{16}H_{20}N_2O_4$) = 304.14. ESI-MS (*m*/*z*): 305.2 (M + H^+). ^{1}H NMR (300 MHz, $CDCl_3$) *δ*/ppm: 8.29 (s, 1H), 8.07 (d, *J* = 7.8 Hz, 1H), 7.99 (d, *J* = 7.8 Hz, 1H), 7.50 (t, *J* = 7.8 Hz, 1H), 6.77 (d, *J* = 6.6 Hz, 1H), 4.82 (quin., *J* = 7.2 Hz, 1H), 4.14 (s, 2H), 3.79 (s, 3H), 1.53 (d, *J* = 7.2 Hz, 3H), 1.40 (s, 6H). ^{13}C NMR (151 MHz, $CDCl_3$) *δ*/ppm: 173.64, 166.17, 161.46, 134.25, 131.47, 130.61, 128.94, 128.57, 126.24, 79.42, 67.94, 52.71, 48.70, 28.54, 28.52, 18.67. ESI-HRMS (*m*/*z*): expected 305.15, 327.13 ($C_{16}H_{20}N_2O_4$ + H^+, $C_{16}H_{20}N_2O_4$ + Na^+), observed 305.1492, 327.1307. IR (KBr): 3344 (w), 2970 (w), 1745 (m), 1650 (s), 1166 (m), 1540 (m), 1213 (m), 1064 (w), 973 (w), 712 (m).

(Me$_2$-ox)-*p*C$_6$H$_4$-Ala (1$_p$). AMP-*p*C_6H_4-Ala (**3p1**) (0.4 mmol). Chromatography: 30 g of silica gel, hexane: ethyl acetate = 3 : 7. Yield: 62.1 mg (0.2 mmol, 57%), yellow powder. M_r ($C_{16}H_{20}N_2O_4$) = 304.14. ESI-MS (*m*/*z*): 305.1 (M + H^+). ^{1}H NMR (300 MHz, $CDCl_3$) *δ*/ppm: 8.01 (d, *J* = 8.5 Hz, 2H), 7.83 (d, *J* = 8.5 Hz, 2H), 6.76 (d, *J* = 6.5 Hz, 1H), 4.81 (quin., *J* = 7.2 Hz, 1H), 4.13 (s, 2H), 3.80 (s, 3H), 1.54 (d, *J* = 7.1 Hz, 3H), 1.40 (s, 6H). ^{13}C NMR (75 MHz, $CDCl_3$) *δ*/ppm: 173.75, 166.19, 161.53–161.03 (m), 136.22, 131.30, 128.61, 127.16, 79.42, 68.00, 52.78, 48.71, 28.52, 18.77. ESI-HRMS (*m*/*z*): expected 305.15, 327.13, 631.27 ($C_{16}H_{20}N_2O_4$ + H^+, $C_{16}H_{20}N_2O_4$ + Na^+, 2($C_{16}H_{20}N_2O_4$) + Na^+), observed 305.1492, 327.1307, 631.2725. IR (KBr): 3273 (s), 3195 (m), 1654 (s), 1858 (m), 1534 (s), 1455 (m), 1368 (m), 1296 (m), 1038 (m), 759 (m), 608 (w), 533 (w), 442 (w).

(H$_2$-ox)-*m*C$_6$H$_4$-Phe (1$_{m2}$). ETA-*m*C_6H_4-Phe (**3$_{m2}$**) (0.8 mmol). Chromatography: 30 g of silica gel, hexane: ethyl acetate = 2 : 8. Yield: 197.8 mg (0.6 mmol, 68%), white solid. M_r ($C_{20}H_{20}N_2O_4$) = 352.14. ESI-MS (*m*/*z*): 353.10 (M + H^+, 100%), 705.25 (2M + H^+, 13%), 727.20 (2M + Na^+, 9%). ^{1}H NMR (600 MHz, $CDCl_3$) *δ*/ppm: 8.27 (t, *J* = 1.8 Hz, 1H), 8.09 (dt, *J* = 7.8, 1.4 Hz, 1H), 7.89 (dt, *J* = 7.7, 1.5 Hz, 1H), 7.49 (t, *J* = 7.8 Hz, 1H), 7.34–7.21 (m, 3H), 7.18–7.10 (m, 2H), 6.63 (d, *J* = 7.6 Hz, 1H), 5.16–5.03 (m, 1H), 4.54–4.32 (m, 2H), 4.09 (t, *J* = 9.5 Hz, 2H), 3.76 (s, 3H), 3.36–3.16 (m, 2H). ^{13}C NMR (151 MHz, CD_3OD) *δ*/ppm: 173.52, 169.26, 166.18, 138.48, 135.82, 132.20, 131.55, 130.22, 129.88, 129.53, 128.25, 127.88, 69.32, 55.96, 55.28, 52.79, 38.14. MALDI-HRMS (*m*/*z*): expected 353.15 ($C_{20}H_{20}N_2O_4$ + H^+), observed 353.1704. IR (ATR): 3273 (w), 2954 (m), 1759 (w), 1737 (m), 1646 (m), 1541 (m), 1439 (m), 1275 (m), 1256 (m), 1183 (m), 950 (m), 702 (m).

(i-Pr-ox)-*m*C$_6$H$_4$-Ala (1$_{m3}$). Val$^{\#}$-*m*C_6H_4-Ala (**3$_{m3}$**) (0.5 mmol). Chromatography: 40 g of silica gel, hexane: ethyl acetate = 7 : 3. Yield: 74.3 mg (0.2 mmol, 47%), white solid. M_r ($C_{17}H_{22}N_2O_4$) = 318.16. ESI-MS (*m*/*z*): 319.15 (M + H^+, 100%). ^{1}H NMR (300 MHz, $CDCl_3$) *δ*/ppm: 8.32 (s, 1H), 8.04 (ddt, *J* = 31.8, 7.7, 1.5 Hz, 2H), 7.50 (t, *J* = 7.8 Hz, 1H), 6.80 (d, *J* = 7.3 Hz, 1H), 4.82 (quin., *J* = 7.2 Hz, 1H), 4.44 (td, *J* = 7.3, 2.1 Hz, 1H), 4.23–4.00 (m, 2H), 3.79 (s, 3H), 1.87 (quin, *J* = 6.6 Hz, 1H), 1.54 (d, *J* = 7.2 Hz, 3H), 1.04 (d, *J* = 6.7 Hz, 3H), 0.94 (d, *J* = 6.7 Hz, 3H). ^{13}C NMR (151 MHz, CD_3OD) *δ*/ppm: 174.73, 169.20, 165.23, 135.76, 132.30, 131.65, 131.64, 129.92, 129.12, 128.42, 73.29, 71.55, 52.81, 50.18, 33.82, 18.84, 18.19, 17.21. MALDI-HRMS (*m*/*z*): expected 637.32 (2($C_{16}H_{20}N_2O_4$) + H^+), observed 637.3234. IR (ATR): 3312 (w), 2961 (w), 1741 (m), 1644 (m), 1536 (m), 1448 (m), 1213 (m), 1169 (m), 967 (m), 788 (m), 704 (m).

(Bzn-ox)-*m*C$_6$H$_4$-Ala (1$_{m4}$). Phe$^{\#}$-*m*C_6H_4-Ala (**3$_{m4}$**) (0.9 mmol). Column chromatography (silica 40g), EtOAc: hexane = 3 : 7 → EtOAc: hexane = 1 : 1. Yield: 226,2 mg (0.6 mmol, 67%), white solid. M_r ($C_{21}H_{22}N_2O_4$) = 366.16. ESI-MS (*m*/*z*): 367.15 (M + H^+, 100%), 733.25 (2M + H^+, 11%). ^{1}H NMR (300 MHz, $CDCl_3$) *δ*/ppm: 8.31 (t, *J* = 1.8 Hz, 1H), 8.04 (ddt, *J* = 26.5, 7.9, 1.5 Hz, 2H), 7.51 (t, *J* = 7.8 Hz, 1H), 7.40–7.19 (m, 5H), 6.80 (d, *J* = 7.3 Hz, 1H), 4.82 (quin., *J* = 7.2 Hz, 1H), 4.70–4.53 (m, 1H), 4.27 (dt, 2H), 3.79 (s, 3H), 3.32–2.65 (m, 2H), 1.54 (d, *J* = 7.2 Hz, 3H). ^{13}C NMR (151 MHz, $CDCl_3$) *δ*/ppm: 173.66, 166.20, 163.44, 137.89, 134.31, 131.50, 130.71, 129.38, 128.99, 128.82, 128.74, 128.22, 126.75, 126.42, 72.23, 68.04, 52.71, 48.72, 41.88, 18.64. MALDI-HRMS (*m*/*z*): expected 367.1658, 389.1469 ($C_{21}H_{22}N_2O_4$ + H^+, $C_{21}H_{22}N_2O_4$ + Na^+), observed 367.1649, 389.1469. IR (ATR): 3317 (w), 2960 (w), 1735 (m), 1649 (m), 1528 (m), 1265 (m), 1210 (m), 1165 (m), 972 (m), 734 (m), 700 (s).

(Ph-ox)-*m*C$_6$H$_4$-Ala (1$_{m5}$). Phg$^{\#}$-*m*C_6H_4-Ala (**3$_{m5}$**) (0.5 mmol). Flash chromatography, prepacked silicagel column, EtOAc: hexane = 1 : 1 → pure EtOAc. Yield: 66.6 mg (0.2 mmol, 36%), colorless oil. M_r ($C_{20}H_{20}N_2O_4$) = 352.14. ESI-MS (*m*/*z*): 353.10 (M + H^+, 100%), 705.25 (2M + H^+, 17%), 727.20 (2M + Na^+, 9%). ^{1}H NMR (300 MHz, $CDCl_3$) *δ*/ppm: 8.43 (t, *J* = 1.8 Hz, 1H), 8.10 (ddt, *J* = 38.6, 7.8, 1.5 Hz, 2H), 7.54 (t, *J* = 7.8 Hz, 1H), 7.42–7.18 (m, 5H), 6.85 (d, *J* = 7.4 Hz, 1H), 5.41 (dd, *J* = 10.2, 8.2 Hz, 1H), 4.93–4.76 (m, 2H), 4.32 (t, *J* = 8.3 Hz, 1H), 3.78 (s, 3H), 1.53 (d, *J* = 7.2 Hz, 3H), 1.26 (t, 2H). ^{13}C NMR (151 MHz, $CDCl_3$) *δ*/ppm: 173.63, 166.12, 164.14, 142.10, 134.32, 131.66, 130.96, 129.04, 128.98, 127.97, 127.93, 126.90, 126.86, 126.57, 75.20, 70.35, 52.69, 48.74, 48.70, 18.58. MALDI-HRMS (*m*/*z*): expected 353.1501, 375.1315 ($C_{20}H_{20}N_2O_4$ + H^+, $C_{20}H_{20}N_2O_4$ + Na^+), observed 353.1493, 375.1316. IR (ATR): 3291 (w), 2954 (w), 1737 (m), 1638 (s), 1536 (m), 1265 (m), 1211 (m), 1169 (m), 699 (s).

(Ph-ox)-*m*C$_6$H$_4$-Gly–Val–Phe (1$_{m6}$). Phg$^{\#}$-*m*C_6H_4-Gly–Val–Phe (**3$_{m6}$**) (1.0 mmol). Column chromatography (silica 50 g), 2% → 5% MeOH in DCM. Yield: 276,5 mmol, 47%), white solid. M_r ($C_{33}H_{36}N_4O_6$) = 584.26. ESI-MS (*m*/*z*): 585.2 (M + H^+, 100%), 1169.5(2M + H^+, 4%). ^{1}H NMR (300 MHz, $CDCl_3$) *δ*/ppm: 8.46 (t, *J* = 1.8 Hz, 1H), 8.21–8.10 (m, 1H), 8.08–7.98 (m, 1H), 7.52 (t, *J* = 7.8 Hz, 1H), 7.45–7.15 (m, 9H), 7.09 (dd, *J* = 7.9, 1.7 Hz, 2H), 6.67 (d, *J* = 8.7 Hz, 1H), 6.55 (d, *J* = 8.0 Hz, 1H), 5.39 (dd, *J* = 10.1, 8.2 Hz, 1H), 4.92–4.74 (m, 2H), 4.37–4.23 (m, 2H), 4.08 (dd, *J* = 8.8, 5.2 Hz, 2H), 3.68 (s, 3H), 3.19–2.98 (m, 2H), 2.17–2.00 (m, 1H), 0.88 (dd, *J* = 16.0, 6.8 Hz, 6H). ^{1}H NMR (600 MHz, DMSO) *δ*/ppm: 8.95 (t, *J* = 6.0 Hz, 1H), 8.48 (m, 2H), 8.11–8.03 (m, 2H), 7.81 (d, *J* = 9.1 Hz, 1H), 7.63 (t, *J* = 7.8 Hz, 1H), 7.43–7.15 (m, 10H), 5.45 (dd, *J* = 10.1, 8.1 Hz, 1H), 4.92–4.84 (m,

1H), 4.45 (ddd, J = 8.8, 7.2, 6.2 Hz, 1H), 4.25 (m, 2H), 3.93 (d, J = 6.0 Hz, 2H), 3.54 (s, 3H), 3.06–2.88 (m, 2H), 1.94 (h, J = 6.8 Hz, 1H), 0.81 (dd, J = 28.8, 6.8 Hz, 6H). ^{13}C NMR (75 MHz, CD_3OD) δ/ppm: 173.46, 173.18, 171.50, 169.43, 166.31, 143.33, 138.10, 135.74, 132.53, 132.28, 132.06, 131.96, 130.26, 130.09, 129.90, 129.54, 129.50, 128.93, 128.87, 128.57, 128.48, 128.07, 127.86, 76.60, 70.94, 59.89, 57.96, 55.25, 52.59, 44.15, 38.31, 32.00, 19.63, 18.38. MALDI-HRMS (m/z): expected 585.27 ($C_{33}H_{36}N_4O_6$ + H^+), observed 585.2736. IR (KBr): 3408 (m), 3304 (m), 3065 (m), 2966 (m), 1745 (m), 1650 (s), 1538 (s), 1270 (m), 1235 (m), 1216 (m), 1075 (m), 957 (m), 762 (m), 701 (s), 544 (w).

(Ph-ox)$_2$-*m*C$_6$H$_4$ (1$_{m7}$). (Phg$^{\#}$)$_2$-*m*C$_6$H$_4$ (**4$_{m4}$**) (0.3 mmol). Column chromatography (silica 20 g), 2% → 5% MeOH in DCM. Yield: 24.3 mg (0.1 mmol, 22%), white solid. M_r ($C_{24}H_{20}N_2O_2$) = 368.15. ESI-MS (m/z): 369.15 (M + H^+, 100%), 737.25 (2M + H^+, 15%). ^{1}H NMR (300 MHz, $CDCl_3$) δ/ppm: 8.69 (d, J = 1.8 Hz, 1H), 8.20 (dd, J = 7.8, 1.7 Hz, 2H), 7.52 (t, J = 7.8 Hz, 1H), 7.42–7.24 (m, 10H), 5.41 (dd, J = 10.1, 8.2 Hz, 2H), 4.82 (dd, J = 10.2, 8.5 Hz, 2H), 4.30 (t, J = 8.3 Hz, 2H).^{13}C NMR (151 MHz, CD_3OD) δ/ppm: 166.18, 143.29, 132.76, 130.25, 129.90, 129.42, 129.04, 128.91, 127.84, 76.63, 70.93. MALDI-HRMS (m/z): expected 369.15 ($C_{24}H_{20}N_2O_2$ + H^+), observed 369.1810. IR (ATR): 2904 (w), 1649 (m), 1456 (m), 1347 (m), 1267 (m), 1236 (m), 1079 (m), 980 (m), 958 (m), 760 (m), 695 (s).

(Me$_2$-ox)-1,4-Nph-Ala (1$_{n1}$). AMP-1,4-Nph-Ala (**3$_{n1}$**) (0.5 mmol). Chromatography: 35 g of silica gel, hexane: ethyl acetate = 1 : 1. Yield: 74.3 mg (0.2 mmol, 42%), white powder. M_r ($C_{20}H_{22}N_2O_4$) = 354.16. ESI-MS (m/z): 355.2 (M + H^+), 709.4 (2M + H^+). ^{1}H NMR (600 MHz, $CDCl_3$) δ/ppm: 9.08 (d, J = 8.2 Hz, 1H), 8.33 (d, J = 7.9 Hz, 1H), 8.01 (d, J = 7.4 Hz, 1H), 7.66–7.56 (m, 3H), 6.53 (d, J = 7.3 Hz, 1H), 4.92 (quin., J = 7.2 Hz, 1H), 4.17 (s, 2H), 3.83 (s, 3H), 1.61–1.57 (m, 3H), 1.49 (s, 6H). ^{13}C NMR (151 MHz, $CDCl_3$) δ/ppm: 173.47, 168.78, 161.45, 136.97, 131.59, 130.49, 127.82, 127.69, 127.66, 127.40, 126.80, 125.70, 123.91, 78.58, 68.78, 52.78, 48.72, 28.67, 18.59. ESI-HRMS (m/z): expected 355.17, 377.15, 393.12 ($C_{20}H_{22}N_2O_4$ + H^+, $C_{20}H_{22}N_2O_4$ + Na^+, $C_{20}H_{22}N_2O_4$ + K^+), observed 355.1643, 377.1463, 393.1202.

(Me$_2$-ox)-1,4-Nph-Gly (1$_{n2}$). AMP-1,4-Nph-Gly (**3$_{n2}$**) (1.0 mmol). Chromatography: 40 g of silica gel, hexane: ethyl acetate = 1 : 1. Yield: 119.9 mg (0.4 mmol, 35%), white powder. M_r ($C_{19}H_{20}N_2O_4$) = 340.14. ESI-MS (m/z): 341.1 (M + H^+). ^{1}H NMR (300 MHz, $CDCl_3$) δ/ppm: 9.12–9.01 (m, 1H), 8.41–8.28 (m, 1H), 8.01 (d, J = 7.4 Hz, 1H), 7.69–7.55 (m, 3H), 6.55 (t, J = 5.0 Hz, 1H), 4.34 (d, J = 5.4 Hz, 2H), 4.17 (s, 2H), 3.83 (s, 3H), 1.49 (s, 6H). ^{13}C NMR (151 MHz, CD_3OD) δ/ppm: 172.34, 171.68, 164.53, 138.67, 132.37, 131.64, 128.63, 128.59, 128.34, 127.12, 127.00, 125.08, 80.22, 69.24, 52.74, 42.28, 28.53. ESI-HRMS (m/z): expected 341.15, 363.13, 379.11 ($C_{19}H_{20}N_2O_4$ + H^+, $C_{19}H_{20}N_2O_4$ + Na^+, $C_{19}H_{20}N_2O_4$ + K^+), observed 341.1488, 363.1305, 379.1045. IR (KBr): 3447 (w), 3300 (m), 2970 (w), 1736 (s), 1643 (m), 1528 (m), 1324 (w), 1276 (m), 1246 (m), 1113 (w), 1008 (w), 1004 (w), 865 (w), 778 (w).

(Me$_2$-ox)-1,5-Nph-Ala (1$_{n3}$). AMP-1,5-Nph-Ala (**3$_{n3}$**) (1.0 mmol). Chromatography: 35 g of silica gel, hexane: ethyl acetate = 35 : 65. Yield: 147.1 mg (0.4 mmol, 42%), white powder. M_r ($C_{20}H_{22}N_2O_4$) = 354.16. ESI-MS (m/z): 355.1 (M + H^+). ^{1}H NMR (300 MHz, $CDCl_3$) δ/ppm: 9.19 (d, J = 8.6 Hz, 1H), 8.47 (d, J = 8.6 Hz, 1H), 8.11–8.04 (m, 1H), 7.72–7.65 (m, 1H), 7.61–7.52 (m, 2H), 6.56 (d, J = 7.3 Hz, 1H), 4.91 (quin., J = 7.2 Hz, 1H), 4.16 (s, 2H), 3.82 (s, 3H), 1.59 (d, 3H), 1.48 (s, 6H). ^{13}C NMR (75 MHz, $CDCl_3$) δ/ppm: 134.25, 131.55, 130.56, 129.41, 129.36, 128.99, 126.06, 126.05, 125.54, 125.44, 78.51, 68.66, 52.75, 48.71, 28.69, 18.61. ESI-HRMS (m/z): expected 355.17, 377.15, 731.31 ($C_{20}H_{22}N_2O_4$ + H^+, $C_{20}H_{22}N_2O_4$ + Na^+, 2($C_{20}H_{22}N_2O_4$) + Na^+), observed 355.1642, 377.1461, 731.3026. IR (KBr): 3421 (w), 3341 (w), 2969 (w), 1745 (m), 1642 (m), 1528 (w), 1215 (w), 1197 (w), 1160 (w), 1040 (w), 797 (w).

(Me$_2$-ox)-2,6-Nph-Ala (1$_{n4}$). AMP-2,6-Nph-Ala (**3$_{n4}$**) (0.5 mmol). Chromatography: 30 g of silica gel, hexane: ethyl acetate = 6 : 4, ratio gradually changed to 1 : 1. Yield: 76.3 mg (0.2 mmol, 43%), white powder. M_r ($C_{20}H_{22}N_2O_4$) = 354.16. ESI-MS (m/z): 355.2 (M + H^+), 709.3 (2M + H^+). Crystals suitable for single-crystal X-ray diffraction were obtained from solution in NMR tube after several months. ^{1}H NMR (600 MHz, $CDCl_3$) δ/ppm: 8.47 (s, 1H), 8.32 (s, 1H), 8.09 (d, J = 8.6 Hz, 1H), 7.95 (t, J = 8.4 Hz, 2H), 7.89 (d, J = 8.4 Hz, 1H), 6.89 (d, J = 6.8 Hz, 1H), 4.87 (quin., J = 7.1 Hz, 1H), 4.18 (s, 2H), 3.82 (s, 3H), 1.57 (d, J = 7.1 Hz, 3H), 1.43 (s, 6H). ^{13}C NMR (151 MHz, $CDCl_3$) δ/ppm: 173.82, 166.73, 161.96, 134.30, 133.94, 132.68, 129.56, 129.17, 128.45, 127.47, 127.34, 125.99, 124.40, 79.45, 67.98, 52.78, 48.77, 28.59, 18.82. ESI-HRMS (m/z): expected 355.17, 377.15, 731.31 ($C_{20}H_{22}N_2O_4$ + H^+, $C_{20}H_{22}N_2O_4$ + Na^+, 2($C_{20}H_{22}N_2O_4$) + Na^+), observed 355.1642, 377.1464, 731.3038. IR (KBr): 3474 (w), 3358 (w), 2973 (w), 1752 (m), 1639 (s), 1523 (m), 1207 (m), 1188 (m), 1161 (m), 1062 (m), 979 (w), 912 (w), 823 (w), 758 (w), 717 (w), 483 (w).

(Me$_2$-ox)-2,7-Nph-Ala (1$_{n5}$). AMP-2,7-Nph-Ala (**3$_{n5}$**) (1.0 mmol). Chromatography: 35 g of silica gel, hexane: ethyl acetate = 1 : 1. Yield: 48.8 mg (0.1 mmol, 14%), white powder. M_r ($C_{20}H_{22}N_2O_4$) = 354.16. ESI-MS (m/z): 355.2 (M + H^+). ^{1}H NMR (300 MHz, $CDCl_3$) δ/ppm: 8.50 (d, J = 1.3 Hz, 1H), 8.37 (s, 1H), 8.17–8.09 (m, 1H), 7.94–7.86 (m, 3H), 6.88 (d, J = 7.3 Hz, 1H), 4.86 (quin., J = 7.2 Hz, 1H), 4.18 (s, 2H), 3.82 (s, 3H), 1.57 (d, J = 7.1 Hz, 3H), 1.43 (s, 6H). ^{13}C NMR (75 MHz, $CDCl_3$) δ/ppm: 173.80, 166.69, 161.90, 136.12, 132.11, 131.99, 129.62, 128.56, 128.51, 128.00, 127.00, 126.59, 125.26, 79.43, 67.96, 52.77, 48.78, 28.59, 18.82. ESI-HRMS (m/z): expected 355.17, 377.15, 731.31 ($C_{20}H_{22}N_2O_4$ + H^+, $C_{20}H_{22}N_2O_4$ + Na^+, 2($C_{20}H_{22}N_2O_4$) + Na^+), observed 355.1645, 377.1464, 731.3037. IR (KBr): 3444 (w), 3260 (w), 3045 (w), 2978 (w), 1740 (s), 1658 (s), 1637 (m), 1544 (m), 1316 (m), 1228 (m), 1168 (m), 1076 (m), 959 (w), 867 (w), 710 (w).

(Me$_2$-ox)-9,10-Anth-Ala (1$_{a1}$). AMP-9,10-Anth-Ala (**3$_{a1}$**) (0.4 mmol), DAST (0.8 mmol). Chromatography: 20 g of silica gel, 1.5% MeOH in DCM. Yield: 138.7 mg (0.3 mmol, 87%), white powder. M_r ($C_{24}H_{24}N_2O_4$) = 404.17. ESI-MS (m/z): 405.1 (M + H^+). ^{1}H NMR (600 MHz, $CDCl_3$) δ/ppm: 8.32–7.95 (m, 4H), 7.57–7.52 (m, 4H), 6.51 (d, J = 7.4 Hz, 1H), 5.08 (quin., J = 7.3 Hz, 1H), 4.37 (s, 2H), 3.87 (s, 3H), 1.66 (d, J = 7.3 Hz, 3H), 1.64 (s, 6H). ^{13}C NMR (151 MHz, CD_3OD) δ/ppm: 174.61, 171.57, 164.12, 135.91, 130.67, 130.60, 129.01, 128.59, 128.29, 128.18, 127.85, 127.75, 127.27, 126.60, 126.20, 126.00, 125.39, 80.93, 69.67, 52.92, 50.30, 28.80, 16.98. ESI-HRMS (m/z): expected 405.18, 427.16, 831.31 ($C_{24}H_{24}N_2O_4$ + H^+, $C_{24}H_{24}N_2O_4$ + Na^+, 2($C_{20}H_{22}N_2O_4$) + Na^+), observed 405.1802, 427.1621, 831.3346. IR (KBr): 3416

(m), 3229 (m), 3052 (w), 2971 (m), 2926 (w), 1745 (s), 1653 (s), 1541 (s), 1445 (m), 1329 (s), 1529 (m), 1217 (s), 1195 (m), 1160 (m), 1113 (m), 1051 (m), 994 (s), 863 (m), 773 (m), 664 (m), 605 (w).

(Me$_2$-ox)-1,3,5-C$_6$H$_3$-(Ala-OMe)$_2$ ($\mathbf{1_{t1}}$). AMP-1,3,5-C$_6$H$_3$-(Ala-OMe)$_2$ ($\mathbf{3_{t1}}$) (0.7 mmol). Chromatography: 35 g of silica gel, 1% MeOH in DCM. Yield: 266.0 mg (0.6 mmol, 86%), colorless oil. M_r ($C_{21}H_{27}N_3O_7$) = 433.18. ESI-MS (*m*/*z*): 434.2 (M + H$^+$), 867.3 (2M + H$^+$, 19%). ^{1}H NMR (300 MHz, $CDCl_3$) δ/ppm: 8.43 (d, J = 1.7 Hz, 2H), 8.38 (d, J = 1.7 Hz, 1H), 7.01 (d, J = 7.4 Hz, 2H), 4.82 (quin., J = 7.2 Hz, 2H), 4.16 (s, 2H), 3.79 (s, 3H), 1.54 (d, J = 7.2 Hz, 6H), 1.41 (d, J = 2.8 Hz, 6H). ^{13}C NMR (151 MHz, CD_3OD-good) δ/ppm: 174.64, 168.37, 163.18, 136.31, 131.08, 130.49, 129.74, 80.76, 68.88, 52.85, 50.26, 28.41, 17.23. MALDI-HRMS (*m*/*z*): expected 434.18 ($C_{21}H_{27}N_3O_7$ + H$^+$), observed 434.2037. IR (KBr): 3393 (m), 2971 (w), 1742 (s), 1656 (s), 1540 (s), 1455 (m), 1213 (m), 1164 (m), 1096 (w), 1054 (w), 979 (m), 721 (m).

(i-Pr-ox)-1,3,5-C$_6$H$_3$-(Gly-OMe)$_2$ ($\mathbf{1_{t2}}$). HO-Val-1,3,5-C$_6$H$_3$-(Gly-OMe)$_2$ ($\mathbf{3_{t2}}$) (0.5 mmol). Chromatography: 30 g of silica gel, hexane: ethyl acetate = 2 : 8. Yield: 28.3 mg (0.1 mmol, 13%), yellow solid. ^{1}H NMR (300 MHz, CD_3CN) δ/ppm: 8.46 (d, J = 1.7 Hz, 2H), 8.38 (s, 1H), 7.93 (s, 1H), 7.62 (s, 2H), 4.50 (s, 1H), 4.27–4.02 (m, 6H), 3.71 (s, 6H), 1.11–0.87 (m, 6H). ^{13}C NMR (151 MHz, CD_3OD) δ/ppm: 171.77, 171.73, 169.02, 168.92, 168.75, 164.31, 137.39, 136.19, 135.98, 132.61, 131.02, 130.41, 130.37, 130.06, 129.85, 73.58, 71.86, 63.36, 63.13, 59.13, 52.75, 52.72, 42.47, 42.46, 33.89, 30.33, 20.09, 19.31, 18.86, 18.34. MALDI-HRMS (*m*/*z*): expected 420.19 ($C_{20}H_{25}N_3O_7$ + H$^+$), observed 420.1796. IR (ATR): 3315 (w), 2961 (w), 2930 (w), 1741 (m), 1655 (m), 1534 (m), 1219 (m), 1088 (m), 734 (s), 704 (m).

(Ph-ox)-1,3,5-C$_6$H$_3$-(L-Phe-OMe)$_2$ ($\mathbf{1_{t3}}$). Phg$^{\#}$-1,3,5-C$_6$H$_3$-(Phe-OMe)$_2$ ($\mathbf{3_{t3}}$) (0.7 mmol). Chromatography: 20 g of silica gel, hexane : ethyl acetate = 1 : 1. Yield: 168.6 mg (0.3 mmol, 38%), colorless oil. M_r ($C_{37}H_{35}N_3O_7$) = 633.25. ESI-MS (*m*/*z*): 634.1 (M + H$^+$), 1267.3 (2M + H$^+$, 11%). ^{1}H NMR (300 MHz, $CDCl_3$) δ/ppm: 8.47 (d, J = 1.7 Hz, 2H), 8.27 (s, 1H) 7.47–7.03 (m, 15H), 6.74 (d, J = 7.7 Hz, 2H), 5.42 (d, J = 1.8 Hz, 1H), 5.09 (dt, J = 7.8, 6.0 Hz, 2H), 4.85 (dd, J = 10.2, 8.5 Hz, 1H), 4.33 (t, J = 8.4 Hz, 1H), 3.75 (s, 6H), 3.25 (qd, J = 13.9, 6.0 Hz, 4H). ^{13}C NMR (75 MHz, $(CD_3)_2CO$) δ/ppm: 172.85, 166.24, 163.74, 143.74, 138.47, 135.97, 130.46, 130.25, 130.15, 129.59, 129.46, 129.34, 128.43, 127.76, 127.62, 76.00, 71.01, 55.52, 52.51, 38.02. MALDI-HRMS (*m*/*z*): expected 634.26 ($C_{37}H_{35}N_3O_7$ + H$^+$), observed 634.2578. IR (ATR): 3312 (w), 3032 (w), 2954 (w), 1737 (m), 1655 (s), 1524 (m), 1215 (m), 1100 (m), 980 (m), 734 (m), 699 (s).

(Ph-ox)-1,3,5-C$_6$H$_3$-(D-Phe-OMe)$_2$ ($\mathbf{1_{t4}}$). Phg$^{\#}$-1,3,5-C$_6$H$_3$-(D-Phe-OMe)$_2$ ($\mathbf{3_{t4}}$) (1.0 mmol). Chromatography: 30 g of silica gel, hexane : ethyl acetate = 1 : 1. Yield: 363.0 mg (0.6 mmol, 57%), white solid. M_r ($C_{37}H_{35}N_3O_7$) = 633.25. ESI-MS (*m*/*z*): 634.2 (M + H$^+$), 1267.4 (2M + H$^+$, 13%). ^{1}H NMR (300 MHz, CD_3CN) δ/ppm: 8.42 (d, J = 1.7 Hz, 2H), 8.21 (t, J = 1.8 Hz, 1H), 7.50 (d, J = 8.0 Hz, 2H), 7.45–7.11 (m, 15H), 5.43 (dd, J = 10.1, 8.1 Hz, 1H), 4.92-4.85 (m, 3H), 4.27 (t, J = 8.3 Hz, 1H), 3.69 (s, 6), 3.39–3.00 (m, 4H). ^{13}C NMR (151 MHz, CD_3OD) δ/ppm: 173.44, 168.40, 165.47, 143.22, 138.36, 136.38, 131.10, 130.75, 130.22, 129.90, 129.57, 129.31, 128.94, 127.92, 127.86, 76.73, 71.06, 56.03, 52.84, 38.20. IR (KBr): 3419 (m), 3030 (w), 2953 (w), 2493 (w), 1742 (s), 1660 (s), 1600 (m), 1455 (s), 1435 (s), 1410 (m), 1357 (m), 1234 (m), 1204 (m), 1180 (m), 1100 (m), 983 (m), 758 (m), 701 (s).

(Ph-ox)$_2$-1,3,5-C$_6$H$_3$-(L-Phe-OMe) ($\mathbf{1_{t5}}$). (Phg$^{\#}$)$_2$-1,3,5-C$_6$H$_3$-L-Phe-OMe ($\mathbf{4_{t5}}$) (0.5 mmol). Chromatography: 20 g of silica gel, hexane: ethyl acetate = 1 : 1. Yield: 97.9 mg (0.2 mmol, 34%), white solid. M_r ($C_{35}H_{31}N_3O_5$) = 573.23. ESI-MS (*m*/*z*): 574.1 (M + H$^+$), 1147.4 (2M + H$^+$, 13%). ^{1}H NMR (300 MHz, CD_3CN) δ/ppm: 8.63 (d, J = 1.6 Hz, 1H), 8.45 (d, J = 1.6 Hz, 2H), 7.54 (d, J = 8.1 Hz, 1H), 7.45–7.07 (m, 15H), 5.44 (dd, J = 10.1, 8.3 Hz, 2H), 4.89 (dd, J = 10.2, 8.5 Hz, 3H), 4.28 (t, J = 8.4 Hz, 2H), 3.69 (s, 3H), 3.38–2.95 (m, 2H). ^{13}C NMR (151 MHz, CD_3OD) δ/ppm: 173.40, 168.34, 165.43, 143.23, 138.42, 136.70, 131.93, 131.43, 130.23, 129.90, 129.59, 129.56, 128.93, 127.90, 127.84, 76.79, 71.06, 56.02, 52.84, 38.16. MALDI-HRMS (*m*/*z*): expected 574.23 ($C_{35}H_{31}N_3O_5$ + H$^+$), observed 574.2406. IR (ATR): 3312 (w), 3066 (w), 3032 (w), 2954 (w), 2904 (w), 1737 (m), 1655 (m), 1541 (m), 1269 (m), 1215 (m), 980 (m), 734 (m), 697 (s).

(Ph-ox)$_2$-1,3,5-C$_6$H$_3$ ($\mathbf{1_{t6}}$)[53]. (Phg$^{\#}$)$_3$-1,3,5-C$_6$H$_3$ ($\mathbf{5_{t5}}$) (0.5 mmol). Chromatography: 30 g of silica gel, hexane : ethyl acetate = 6 : 4. Yield: 52.8 mg (0.2 mmol, 34%), white solid. M_r ($C_{33}H_{27}N_3O_3$) = 513.21. ESI-MS (*m*/*z*): 514.20 (M + H$^+$, 100%), 1027.4 (2M + H$^+$, 19%). ^{1}H NMR (300 MHz, $CDCl_3$) δ/ppm. 8.84 (s, 3H), 7.59–6.88 (m, 15H), 5.43 (dd, J = 10.2, 8.3 Hz, 3H), 4.83 (dd, J = 10.2, 8.5 Hz, 3H), 4.31 (t, J = 8.4 Hz, 3H). ^{13}C NMR (151 MHz, CD_3OD) δ/ppm: 165.33, 143.21, 132.16, 129.89, 129.86, 128.90, 127.81, 76.82, 71.07. MALDI-HRMS (*m*/*z*): expected 514.21 ($C_{33}H_{27}N_3O_3$ + H$^+$), observed 514.2167. IR (ATR): 2963 (w), 2919 (m), 2851 (m), 1649 (m), 1269 (m), 1236 (m), 965 (m), 915 (m), 699 (s).

((Ph-ox)-*m*C$_6$H$_4$-Val-NH-CH$_2$CH$_2$)$_2$ ($\mathbf{1_b}$). (Phg$^{\#}$-*m*C$_6$H$_4$-Val-NH-CH$_2$CH$_2$)$_2$ ($\mathbf{3_b}$) (0.16 mmol). Chromatography: 20 g of silica gel, 5% MeOH in DCM. Yield: 43.5 mg (0.05 mmol, 34%), white solid. M_r ($C_{46}H_{52}N_6O_6$) = 784.39. ESI-MS (*m*/*z*): 393.4 (1/2M + H$^+$, 100%), 785.3 (M + H$^+$, 30%). ^{1}H NMR (300 MHz, CD_3OD) δ/ppm: 8.46 (s, 2H), 8.15 (d, J = 7.9 Hz, 2H), 8.03 (d, J = 7.8 Hz, 2H), 7.60 (t, J = 7.9 Hz, 2H), 7.43–7.27 (m, 10H), 5.49–5.37 (m, 2H), 4.94 (d, J = 8.7 Hz, 2H), 4.32 (dd, J = 14.9, 8.2 Hz, 4H), 2.14 (d, J = 14.7 Hz, 2H), 1.57 (s, 4H), 1.29 (s, 8H), 1.06–0.95 (m, 12H). ^{13}C NMR (151 MHz, CD_3OD) δ/ppm: 179.46, 176.01, 173.67, 169.28, 143.31, 136.16, 132.40, 132.02, 130.08, 129.92, 128.95, 128.77, 128.54, 127.88, 76.64, 70.94, 61.49, 39.98, 31.83, 27.66, 19.84, 19.27. MALDI-HRMS (*m*/*z*): expected 785.40 ($C_{46}H_{52}N_6O_6$ + H$^+$), observed 785.4015. IR (ATR): 3288 (m), 2963 (w), 2930 (w), 2874 (w), 1630 (m), 1523 (m), 1234 (m), 1070 (m), 960 (m), 697 (m).

X-ray single crystal diffraction

X-ray intensity data for $\mathbf{2_{m1}}$–$\mathbf{1_{n5}}$ were collected at room temperature (293 K) with an Xcalibur or XtaLAB diffractometer using monochromatic Cu-Kα radiation (λ = 1.54184 Å). The data were processed using the CrysalisPro program[54] (unit cell determination and data reduction). The structures were solved with the program SXELXT[55] and refined according to the least-squares procedure (F^2 on all data) by the program

SHELXL-2018.[56] Basic experimental data are given in Tables S7 and S8 of the ESI.† Due to the faster scans used in the measurements of $\mathbf{2_{m1}}$ and $\mathbf{1_{n4}}$, a smaller number of reflections were obtained; however, the quality of the final structural parameters for these compounds remained very high (*R* values, min. and max. electron density, Goodness of fit, *etc.*). The absolute configurations of investigated compounds were known from the synthetic procedures, so the Friedel opposite reflections were not measured. All non-hydrogen atoms are refined in the anisotropic model of atomic displacement parameters (ADP). Terminal phenyl groups in $\mathbf{3_{t3}}$ were treated as rigid rings with the ideal geometry (AFIX 66) and one of them was refined over two disorderly occupied positions (orientations), with refined occupancies of 0.55(2) and 0.45(2), respectively. Rigid body restraints for ADP parameters (RIGU, ISOR) were also used for the carbon atoms of terminal phenyl rings in the structure of $\mathbf{3_{t3}}$. Hydrogen atoms bonded to carbon atoms were treated in the riding rigid body models, *i.e.* their positions were calculated from the positions of carbon atoms. Torsion angles of methyl and hydroxyl groups in all compounds (including the solvent methanol molecule in the structure of $\mathbf{1_{m6}}$) were determined by the best fit to the difference in electron density (HFIX 137 or HFIX 147, respectively). Also, the rigid body restrains (RIGU) for ADP parameters for atoms of the solvent methanol molecule. Exceptions from the rigid body treatment were the hydrogen atoms bonded to the nitrogen atoms of the amide groups, due to their participation in the hydrogen bonds. These atoms were refined free, including their isotropic ADP parameters. Additional N–H distance restraints were used for $\mathbf{1_{m6}}$, $\mathbf{1_{t3}}$ and $\mathbf{1_{t4}}$ structures. The CCDC 2335938–2335948† contains the supplementary crystallographic data for this paper.

DFT calculations

Calculation of NMR parameters and structural ensembles (SE) of low energy conformers of $\mathbf{1_{t1}}$ and supramolecular dimers of $\mathbf{1_{t1}}$ in $CHCl_3$ solution was calculated according to the literature suggested CREST/CENSO workflow in several steps:[57,58]

Generation of SE of monomer conformers of $\mathbf{1_{t1}}$. The starting molecular model was constructed by using Avogadro software,[59] optimized by the UFF force field and then reoptimized by using the xtb software with the GFN2-xTB semi-empirical level of theory.[60] Using the alpb solvent model[61] for $CHCl_3$ and GFN2-xTB level of the theory, the iMTD-GC workflow of the CREST calculation[57] found 1599 conformers within the free energy lower than 5 kcal mol^{-1}. Additionally, during the CREST calculation, the NMR chemical/magnetic ^1H nuclear equivalences were determined. Atom labelling scheme is defined in Fig. S21 (ESI†).

Generation of SE of dimer conformers of $\mathbf{1_{t1}}$. The most stable conformer of $\mathbf{1_{t1}}$, obtained after DFT geometry optimization of monomer SE (see below) was used in the modelling of dimer aggregates expecting to exist in the $CHCl_3$ solution of $\mathbf{1_{t1}}$ by using the Avogadro software.[59] Two types of starting dimer models were constructed: vS1 and vS2 (Fig. S23, ESI†). Model vS1 is obtained by copying the structure of the lowest energy $\mathbf{1_{t1}}$ conformer (CONF1, Fig. S22, ESI†) and placing the copied molecule at the distance of 3 Å above the original molecule, in a stacked position in which two benzene rings are mutually parallel. Additionally, the copied molecule is rotated around the axis perpendicular to benzene rings for 60°. Model vS2 is obtained by copying the same lowest energy conformer CONF1 of $\mathbf{1_{t1}}$ and placing the copied molecule at a distance of 3 Å above the original molecule, in a stacked position (two benzene rings are mutually parallel) and rotating the copied molecule around the axis perpendicular to benzene rings for 180°.

Each starting structural model was used as an input in two independent CREST conformational search jobs,[57] with the aim to find other possible, more stable dimer aggregates of $\mathbf{1_{t1}}$ molecules. These jobs used the NCI-iMTD workflow, *i.e.* iterative meta-dynamic simulations (MTD) with additional ellipsoid wall potential.[57] CREST jobs with vS1 or vS2 starting models ended with 95 or 93 conformers (*i.e.* the structural models of $\mathbf{1_{t1}}$-dimer aggregates) within the energy threshold of 6 kcal mol^{-1}, respectively.

Geometry optimizations and evaluation of free energies. The starting structural ensembles of monomer and dimer structural models (conformers) generated by CREST were further refined by using the CENSO software.[58] Structures were gradually optimized (from crude to very-tight convergence threshold) using r^2scan-3c composite DFT level of theory.[62] During optimizations, the smd solvent model for $CHCl_3$ was included.[63] Thermostatistical contributions to free energy (G_{mRRHO}) were calculated using the Single Point Hessian (SPH) approach for frequencies calculated at the GFN2-xTB level of theory at the final DFT-optimized geometries.[64] During the calculation of the frequencies, the alpb solvent model for $CHCl_3$ was used.[61] The final term for complete free energy *G*, the solvation contribution ($G_{solv.}$), was calculated with the smd solvent model for $CHCl_3$.[63] During optimizations, the checking for identical conformers was included, including the energy criteria that only conformers with ΔG lower than 3.5 kcal mol^{-1} (for 298 K) were used in final optimizations. The free energy G_i for each conformer was then calculated at six different temperatures (233, 253, 273, 293, 298 and 313 K). Final ensembles of 47 monomer conformers and 41 dimer conformers are given in separate files ''calc_mono_1t1.xyz'' and ''calc_dimer_1t1.xyz'' with additional ESI,† respectively, and their free energies *G* at different temperatures are given in Tables S11 and S12 of the ESI,† respectively. Boltzmann averaged free energies of the structural ensembles at different temperatures, as well as separated contributions $\langle G_{gas}\rangle$, $\langle G_{solv.}\rangle$ and $\langle G_{mRRHO}\rangle$, are given in Tables S13 and S14 of the ESI,† respectively.

Calculation of NMR parameters and correlations with experiments. For conformers with a Boltzmann population > 1% in each SE, the ^1H–^1H *J* couplings and ^1H and ^{13}C shieldings were calculated by using the GIAO approach.[49] The NMR parameters were calculated at the standard DFT hybrid level (PBE0-d4 functional and Jensen's pcJ-0 for couplings[65] and pcSseg-2 for shieldings[66]), as recommended by Grimme *et al.*[47] With information obtained from the CREST calculation of chemical/magnetic equivalences of the ^1H nuclei and using

experimentally obtained NMR data of the oxazoline CH_2 protons, the shieldings and J couplings were individually averaged for each temperature data set. At low temperatures (233, 253 and 273 K), the calculated shieldings for these protons were left unaveraged, while at high temperatures (293, 298 and 313 K), the calculated shieldings for this signal were averaged over two GIAO calculated proton shieldings. Averaging of other NMR parameters for fast-exchanging proton groups was performed in a similar fashion. This averaging of chemically equivalent nuclei was performed for each individual conformer in the ensembles. The only difference in averaging of NMR parameters between monomer and dimer ensembles was one additional averaging of chemically identical atoms (or atom pairs) for both $\mathbf{1_{t1}}$ molecules in one dimer.

The final Boltzmann-weighted NMR parameters for each temperature was calculated using the relation:

$$\text{param}^{w} = \Sigma_{\text{conf.}} P_i(T) \cdot \text{param}_{\text{CONF}(i)} \qquad (2)$$

where $\text{param}_{\text{CONF}(i)}$ is the NMR parameter of conformer i in a particular structural ensemble (already averaged for fast-exchanging protons) and $P_i(T)$ is the normalized population of conformer i at temperature T. The population $p_i(T)$ is calculated according to

$$p_i(T) = \text{Exp}(-G_i/kT) \Big/ \sum [\text{Exp}(-G_i/kT)] \qquad (3)$$

where G_i is the free energy of conformer i, calculated at temperature T. In (3), the summation is performed over all conformers in the particular ensemble, and in (2), the summation is taken over conformers having $p_i(T) > 2\%$. The normalized population $P_i(T)$ in (2) is the population $p_i(T)$ multiplied by the factor which constrains the sum of populations $P_i(T)$ in (2) to 1.

Calculated Boltzmann-weighted NMR parameters are given in Tables S16 and S17 (ESI†) for monomer and dimer ensembles, respectively. Fig. S24–S27 (ESI†) show the correlations of the calculated, Boltzmann averaged shieldings (σ_i^c) and experimental shifts (δ_i^o), for monomer and dimer ensembles, respectively. For each correlation, the MAE (mean absolute error) values defined by eqn (1) (see results and discussion)[50] were determined. Amide ^{1}H calculated shifts using eqn (2) are also listed in Tables S16 and S17 (ESI†), as well as its absolute error ($AE = |\delta_i^c - \delta_i^o|$) from the experimental value.

All single-point, geometry optimizations and GIAO calculations used by CREST (version 2.12) and CENSO (version 1.2.0) software were performed by the ORCA software (version 5.0.1).[67] All calculations of averaged NMR parameters and linear regression calculations were performed using Excel software[68] and they are available in two Excel tables in ESI† (NMR_mono_1t1.xlsx and NMR_dimer_1t1.xlsx).

Author contributions

M. B. prepared and characterized the compounds, performed the spectroscopic studies and wrote the manuscript draft. B. P. performed the crystallographic and DFT studies. S. I. K. conceived the study, supervised the experiments and finalized the manuscript. All authors have approved the manuscript.

Conflicts of interest

There are no conflicts to declare.

Acknowledgements

This work was supported by CAT Pharma (KK.01.1.1.04.0013), a project co-financed by the Croatian Government and the European Union through the European Regional Development Fund – the Competitiveness and Cohesion Operational Program; and Cage Cat (IP-2022-10-8456), a project financed by the Croatian Science Foundation. M. B. acknowledges the Croatian Science Foundation for a doctoral scholarship (DOK-2021–02-7366). We thank Dr Zoran Kokan, Dr Natalija Pantalon Juraj and Dr Saša Opačak for their helpful discussions.

References

1 J. A. Frump, *Chem. Rev.*, 1971, **71**, 483–505.
2 G. C. Hargaden and P. J. Guiry, *Chem. Rev.*, 2009, **109**, 2505–2550.
3 R. Connon, B. Roche, B. V. Rokade and P. J. Guiry, *Chem. Rev.*, 2021, **121**, 6373–6521.
4 D. A. Evans, K. A. Woerpel, M. M. Hinman and M. M. Faul, *J. Am. Chem. Soc.*, 1991, **113**, 726–728.
5 T. P. Yoon and E. N. Jacobsen, *Science*, 2003, **299**, 1691–1693.
6 P. Braunstein and F. Naud, *Angew. Chem., Int. Ed.*, 2001, **40**, 680–699.
7 R. Hoogenboom, *Angew. Chem., Int. Ed.*, 2009, **48**, 7978–7994.
8 T. Lorson, M. M. Lübtow, E. Wegener, M. S. Haider, S. Borova, D. Nahm, R. Jordan, M. Sokolski-Papkov, A. V. Kabanov and R. Luxenhofer, *Biomaterials*, 2018, **178**, 204–280.
9 H. Wang, Z. Bai, T. Jiao, Z. Deng, H. Tong, G. He, Q. Peng and G. Chen, *J. Am. Chem. Soc.*, 2018, **140**, 3542–3546.
10 J. Holz, M. Ayerbe García, W. Frey, F. Krupp and R. Peters, *Dalton Trans.*, 2018, **47**, 3880–3905.
11 M. W. Chojnacka, J. A. Adjei, A. J. Lough, G. G. Sacripante and R. A. Gossage, *Z. Naturforsch., B: J. Chem. Sci.*, 2020, **75**, 371–377.
12 C.-L. Liu, L.-P. Zhou, D. Tripathy and Q.-F. Sun, *Chem. Commun.*, 2017, **53**, 2459–2462.
13 Y.-Q. Huang and W.-Y. Sun, *CrystEngComm*, 2018, **20**, 6109–6121.
14 M. Durini, E. Russotto, L. Pignataro, O. Reiser and U. Piarulli, *Eur. J. Org. Chem.*, 2012, 5451–5461.
15 S. Dakovic, L. Liscic-Tumir, S. I. Kirin, V. Vinkovic, Z. Raza, A. Suste and V. Sunjic, *J. Mol. Catal. A: Chem.*, 1997, **118**, 27–31.

16 Y. Liu, Y. Wang, Y. Wang, J. Lu, V. Piñón and M. Weck, *J. Am. Chem. Soc.*, 2011, **133**, 14260–14263.
17 D. Obrecht, C. Abrecht, M. Altorfer, U. Bohdal, A. Grieder, M. Kleber, P. Pfyffer and K. Müller, *Helv. Chim. Acta*, 1996, **79**, 1315–1337.
18 S. Dahiya and R. Dahiya, *Eur. J. Med. Chem.*, 2021, **218**, 113406.
19 K. Arora, P. M. Sherilraj and S. L. Mudavath, *Comprehensive Analytical Chemistry*, Elsevier, 2023, vol. 103, pp. 1–28.
20 S. I. Kirin, H.-B. Kraatz and N. Metzler-Nolte, *Chem. Soc. Rev.*, 2006, **35**, 348–354.
21 N. Pantalon Juraj, T. Tandarić, V. Tadić, B. Perić, D. Moreth, U. Schatzschneider, A. Brozovic, R. Vianello and S. I. Kirin, *Dalton Trans.*, 2022, **51**, 17008–17021.
22 M. Pernar, Z. Kokan, J. Kralj, Z. Glasovac, L.-M. Tumir, I. Piantanida, D. Eljuga, I. Turel, A. Brozovic and S. I. Kirin, *Bioorg. Chem.*, 2019, **87**, 432–446.
23 Z. Kokan and S. I. Kirin, *RSC Adv.*, 2012, **2**, 5729–5737.
24 Z. Kokan, B. Kovačević, Z. Štefanić, P. Tzvetkova and S. I. Kirin, *Chem. Commun.*, 2018, **54**, 2094–2097.
25 C. Saavedra, R. Hernández, A. Boto and E. Álvarez, *J. Org. Chem.*, 2009, **74**, 4655–4665.
26 S. E. Snyder, B.-S. Huang, Y.-T. Chen, H.-S. Lin and J. R. Carey, *Org. Lett.*, 2012, **14**, 3442–3445.
27 Z. Kokan, B. Perić, M. Vazdar, Ž. Marinić, D. Vikić-Topić, E. Meštrović and S. I. Kirin, *Chem. Commun.*, 2017, **53**, 1945–1948.
28 X. Caumes, A. Baldi, G. Gontard, P. Brocorens, R. Lazzaroni, N. Vanthuyne, C. Troufflard, M. Raynal and L. Bouteiller, *Chem. Commun.*, 2016, **52**, 13369–13372.
29 M. Raynal, Y. Li, C. Troufflard, C. Przybylski, G. Gontard, T. Maistriaux, J. Idé, R. Lazzaroni, L. Bouteiller and P. Brocorens, *Phys. Chem. Chem. Phys.*, 2021, **23**, 5207–5221.
30 F. Perlitius, A. Walczak, M. Čonková, G. Markiewicz, J. Harrowfield and A. R. Stefankiewicz, *J. Mol. Liq.*, 2022, **367**, 120511.
31 B. Gong, C. Zheng and Y. Yan, *J. Chem. Crystallogr.*, 1999, **29**, 649–652.
32 Z. Kokan and S. I. Kirin, *Eur. J. Org. Chem.*, 2013, 8154–8161.
33 S. I. Kirin, D. Wissenbach and N. Metzler-Nolte, *New J. Chem.*, 2005, **29**, 1168–1173.
34 G. Xu, Q. Luo, S. Eibauer, A. F. Rausch, S. Stempfhuber, M. Zabel, H. Yersin and O. Reiser, *Dalton Trans.*, 2011, **40**, 8800–8806.
35 S. Opačak, B. Perić, T. Gojšić, A. Čikoš, D. Vikić-Topić and S. I. Kirin, *New J. Chem.*, 2022, **46**, 13275–13285.
36 S. Beheshti, S. Martić and H. Kraatz, *Chem. – Eur. J.*, 2012, **18**, 9099–9105.
37 L. J. Farrugia, *J. Appl. Crystallogr.*, 1997, **30**, 565.
38 J. Bernstein, R. E. Davis, L. Shimoni and N. Chang, *Angew. Chem., Int. Ed. Engl.*, 1995, **34**, 1555–1573.
39 T. Aida, E. W. Meijer and S. I. Stupp, *Science*, 2012, **335**, 813–817.
40 M. W. Powner, J. D. Sutherland and J. W. Szostak, *J. Am. Chem. Soc.*, 2010, **132**, 16677–16688.
41 C. Janiak, *J. Chem. Soc., Dalton Trans.*, 2000, 3885–3896.
42 B. Ishimoto, K. Tonan and S. Ikawa, *Spectrochim. Acta, Part A*, 2000, **56**, 201–209.
43 L. Barišić, M. Čakić, K. A. Mahmoud, Y. Liu, H. Kraatz, H. Pritzkow, S. I. Kirin, N. Metzler-Nolte and V. Rapić, *Chem. – Eur. J.*, 2006, **12**, 4965–4980.
44 M. H. Abraham and R. J. Abraham, *New J. Chem.*, 2017, **41**, 6064–6066.
45 E. S. Stevens, N. Sugawara, G. M. Bonora and C. Toniolo, *J. Am. Chem. Soc.*, 1980, **102**, 7048–7050.
46 M. Bursch, J. Mewes, A. Hansen and S. Grimme, *Angew. Chem., Int. Ed.*, 2022, **61**, e202205735.
47 S. Grimme, C. Bannwarth, S. Dohm, A. Hansen, J. Pisarek, P. Pracht, J. Seibert and F. Neese, *Angew. Chem., Int. Ed.*, 2017, **56**, 14763–14769.
48 C. F. Macrae, I. Sovago, S. J. Cottrell, P. T. A. Galek, P. McCabe, E. Pidcock, M. Platings, G. P. Shields, J. S. Stevens, M. Towler and P. A. Wood, *J. Appl. Crystallogr.*, 2020, **53**, 226–235.
49 R. Ditchfield, *Mol. Phys.*, 1974, **27**, 789–807.
50 P. H. Willoughby, M. J. Jansma and T. R. Hoye, *Nat. Protoc.*, 2014, **9**, 643–660.
51 P. P. Bose, M. G. B. Drew, A. K. Das and A. Banerjee, *Chem. Commun.*, 2006, 3196–3198.
52 A. Desmarchelier, M. Raynal, P. Brocorens, N. Vanthuyne and L. Bouteiller, *Chem. Commun.*, 2015, **51**, 7397–7400.
53 H.-J. Kim, D. Moon, M. S. Lah and J.-I. Hong, *Angew. Chem., Int. Ed.*, 2002, **41**, 3174–3177.
54 CrysAlisPro (Version 1.171.39.46), Rigaku Oxford Diffraction Ltd, Yarnton, Oxfordshire, England., 2018.
55 G. M. Sheldrick, *Acta Crystallogr., Sect. A: Found. Adv.*, 2015, **71**, 3–8.
56 G. M. Sheldrick, *Acta Crystallogr., Sect. C: Struct. Chem.*, 2015, **71**, 3–8.
57 P. Pracht, F. Bohle and S. Grimme, *Phys. Chem. Chem. Phys.*, 2020, **22**, 7169–7192.
58 S. Grimme, F. Bohle, A. Hansen, P. Pracht, S. Spicher and M. Stahn, *J. Phys. Chem. A*, 2021, **125**, 4039–4054.
59 M. D. Hanwell, D. E. Curtis, D. C. Lonie, T. Vandermeersch, E. Zurek and G. R. Hutchison, *J. Cheminf.*, 2012, **4**, 17.
60 C. Bannwarth, E. Caldeweyher, S. Ehlert, A. Hansen, P. Pracht, J. Seibert, S. Spicher and S. Grimme, *WIREs Comput. Mol. Sci.*, 2021, **11**, e1493.
61 S. Ehlert, M. Stahn, S. Spicher and S. Grimme, *J. Chem. Theory Comput.*, 2021, **17**, 4250–4261.
62 S. Grimme, A. Hansen, S. Ehlert and J.-M. Mewes, *J. Chem. Phys.*, 2021, **154**, 064103.
63 A. V. Marenich, C. J. Cramer and D. G. Truhlar, *J. Phys. Chem. B*, 2009, **113**, 6378–6396.
64 S. Spicher and S. Grimme, *J. Chem. Theory Comput.*, 2021, **17**, 1701–1714.
65 F. Jensen, *Theor. Chem. Acc.*, 2010, **126**, 371–382.
66 F. Jensen, *J. Chem. Theory Comput.*, 2015, **11**, 132–138.
67 F. Neese, *Wiley Interdiscip. Rev.: Comput. Mol. Sci.*, 2022, **12**, e1606.
68 Microsoft Corporation, 2018. Microsoft Excel, Available at: **https://office.microsoft.com/excel**.